NASA TECHNICAL NOTE

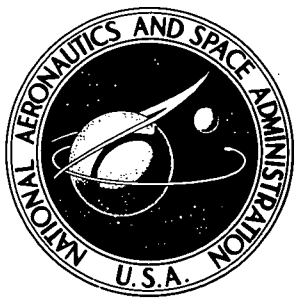

NASA TN D-7234

NASA TN D-7234

ANALYSIS OF INTERNAL FLOW CHARACTERISTICS OF A SMOOTH-DISK WATER-BRAKE DYNAMOMETER

by David G. Evans

Lewis Research Center
Cleveland, Ohio 44135

NATIONAL AERONAUTICS AND SPACE ADMINISTRATION • WASHINGTON, D. C. • MAY 1973

1. Report No.	2. Government Accession No.	3. Recipient's Catalog No.
NASA TN D-7234		

4. Title and Subtitle	5. Report Date
ANALYSIS OF INTERNAL FLOW CHARACTERISTICS OF A SMOOTH-DISK WATER-BRAKE DYNAMOMETER	May 1973
	6. Performing Organization Code

7. Author(s)	8. Performing Organization Report No.
David G. Evans	E-7120
	10. Work Unit No.
	501-24

9. Performing Organization Name and Address	11. Contract or Grant No.
Lewis Research Center National Aeronautics and Space Administration Cleveland, Ohio 44135	
	13. Type of Report and Period Covered
12. Sponsoring Agency Name and Address	Technical Note
National Aeronautics and Space Administration Washington, D.C. 20546	14. Sponsoring Agency Code

15. Supplementary Notes

16. Abstract

The principal of absorbing power with an enclosed partially submerged rotating disk through the turbulent viscous shearing of water is discussed. Reference information is used to develop a flow model of the water brake. A method is then presented that uses vector diagrams to relate the effects of rotational flow, through flow, and secondary flow to power absorption. The method is used to describe the operating characteristics of an example 111-cm (43.7-in.) diameter water brake. Correlating performance parameters are developed in a dimensional analysis.

17. Key Words (Suggested by Author(s))	18. Distribution Statement
Water brake; Dynamometer; Enclosed rotating smooth disk; Dimensional analysis; Fluid mechanics	Unclassified - unlimited

19. Security Classif. (of this report)	20. Security Classif. (of this page)	21. No. of Pages	22. Price*
Unclassified	Unclassified	52	$3.00

* For sale by the National Technical Information Service, Springfield, Virginia 22151

CONTENTS

	Page
SUMMARY	1
INTRODUCTION	1
DESCRIPTION OF WATER BRAKE	2
GENERAL PERFORMANCE EQUATIONS	3
INTERNAL FLOW ANALYSIS	6
PERFORMANCE DATA	8
Kleinsorge	9
Daily and Asbedian (ref. 2)	9
Watabe (ref. 3)	9
Deavers (ref. 4)	10
Ketola and McGrew (ref. 5)	10
Wosika (ref. 6)	10
COMPARISON OF FLOW MODEL WITH DATA	10
Effect of Through Flow	11
Effect of Rotative Speed	12
Example Operating Point For Kleinsorge Water Brake	14
SUMMARY OF RESULTS	16
APPENDIXES	
A - SYMBOLS	18
B - DIMENSIONAL ANALYSIS	20
C - SAMPLE PROBLEM: EFFECT OF THROUGH FLOW	23
D - SAMPLE PROBLEM: EFFECT OF ROTATIVE SPEED	27
E - COMPUTATION OF KLEINSORGE OPERATING POINTS	30
F - COMPUTATION OF VELOCITY DIAGRAMS FOR THE KLEINSORGE WATER BRAKE	32
REFERENCES	39

ANALYSIS OF INTERNAL FLOW CHARACTERISTICS OF A SMOOTH-DISK WATER-BRAKE DYNAMOMETER

by David G. Evans

Lewis Research Center

SUMMARY

Presented is a physical description of a smooth-disk water brake, its method of operation, its performance characteristics, and a review of some of the supporting information available in the literature and from users and manufacturers of water brakes. Test results and data are included. A development of the various parameters and performance prediction equations is made by means of a dimensional analysis of the primary quantities involved.

Also included is a proposed method for representing the various flows that occur within a water brake with vector diagrams, and then comparisons are made between the results from these diagrams and the measured performance. The results indicated that close agreement can be achieved between the vector diagram representation of the internal flow mechanisms of rotational flow, through flow, and secondary flow, with the experimental results on smooth disks noted in the references, and with two water-brake operating points. The flow regime under which the water brake operates is categorized as a smooth disk operating partially submerged with turbulent separated boundary layers (Reynolds number, $\sim 10^8$; disk-to-housing spacing ratio, 0.05).

INTRODUCTION

An analysis is made of the internal flow mechanisms involved in the operation of a smooth-disk type of water-brake dynamometer, sometime referred to as a smooth-disk viscous shear dynamometer. This type of power absorber is applicable to many types of gas turbine component test facilities. It offers the advantages of lower cost and smaller size than electric or pneumatic power absorbers, and offers higher speeds and longer life, quieter, and more cavitation-free operation than drilled-disk or vaned water brakes. These advantages of the smooth-disk water brake over the drilled-disk

or vaned type of water brake are obtained by virtue of the fact that power is absorbed through the viscous shearing of water rather than through the formation of turbulent hydraulic currents or shed eddys, which inherently lead to intense cavitation and damage.

Considerable information is available in the literature concerning the performance characteristics of smooth disks rotating fully submerged in water (or other fluids) in an enclosed housing. Much of this information, even through developed for other types of applications, can be used to describe the operation of a smooth-disk water brake. However, there are aspects of the water brake that are uniquely different. For instance, smooth-disk water brakes operate with partially submerged disks, with through flow, and at substantially higher disk speeds than considered in the references.

Therefore, a study was made to develop a flow model that would effectively describe the operation of a smooth disk at conditions representative of a water brake. Vector diagrams that describe the direction and magnitude of the flow on the disk and housing walls are constructed and analyzed. The diagrams are constructed from test results obtained from a reference 46.0-centimeter (18.1-in.) smooth disk that had been operated fully submerged in air and in water. The diagrams are then modified to represent the operating conditions for an 111-centimeter (43.7-in.) smooth-disk water brake. The effects of core rotational speed, through flow, and secondary flow on water depth, water pressure, and power absorption are considered in the analysis. Where possible, the results are compared with the reference information and with information supplied from the manufacturers and users of water brakes. Also, a dimensional analysis is presented, and the resultant parameters are compared with the vector diagrams, the information noted in the smooth-disk references, and the performance characteristics of the water brakes noted herein.

The information developed in this report was the result of a NASA-Lewis in-house study of water brakes made during a period when consideration was being given to the procurement of a large water brake capable of absorbing 59 600 kilowatts (80 000 hp) at 6000 rpm. Correlation of existing data from the literature presented herein was done as a part of a postgraduate course taken by the author. There is no experience as such in the design or operation of smooth-disk water brakes at the Lewis Research Center.

DESCRIPTION OF WATER BRAKE

The principle of operation of the smooth-disk water brake is to absorb the mechanical energy of rotation through the viscous shearing of water located between a driven rotating disk and a stationary housing. The surfaces of both the disk and housing in contact with the water are smooth. A general layout of the geometry of the water brake and the important dimensions and terms are shown in figure 1 and appendix A.

The frictional drag of an enclosed smooth disk rotating in a fluid has been studied by a number of investigators. In these investigations the interaction of the disk, fluid, and containment has been categorized as occurring in the following four flow regimes:

(I) Laminar - merged wall and disk boundary layers ($Re < 10^5$, $(s/a) < 0.03$)

(II) Laminar - separate wall and disk boundary layers ($Re < 10^5$, $(s/a) > 0.03$)

(III) Turbulent - merged wall and disk boundary layers ($Re > 10^6$, $(s/a) < 0.04$)

(IV) Turbulent - separate wall and disk boundary layers ($Re > 10^6$, $(s/a) > 0.04$).

As noted, the applicable flow regime is dependent on the particular Reynolds number Re and spacing ratio s/a (the approximate range of these values is shown in the parenthetical for each flow regime). For water brakes, Re is of the order of 10^8 and spacing ratio 0.05, which places the water brake in flow regime IV, the turbulent separate boundary-layer regime.

In a water brake the disk is only partially submerged in water. The water is distributed in an annular ring, referred to as a water annulus, which is located between the disk and housing walls. Within the water annulus is a core region, which is shown in figure 2 as the region surrounded by the disk and housing boundary layers. The relative motion between the disk and housing causes the core to rotate at tangential speeds approximately half the disk speed, and this motion is referred to as rotational flow. The viscous shearing of the water, referred to as viscous flow, occurs within the disk and housing wall boundary layers. In addition, the space between the disk and housing s is large enough to allow a secondary flow of water to exist within the core (shown as Q_s in fig. 2). Finally, superimposed on these flows is the radial flow of water through the core caused by the through flow of cold incoming water wt_q or Q (both terms are used herein and in the literature) and its discharge from the water brake after it has been heated by the energy exchange between the disk and housing.

GENERAL PERFROMANCE EQUATIONS

The force F required to shear a fluid between two surfaces is related to the difference in velocity ΔU between the two surfaces, the surface area A_w of the two surfaces, the distance between the surfaces h, and the shear stress τ, kinematic viscosity ν, and mass density φ of the fluid as follows:

$$F = \tau A_w = C_1 \rho A_w (\Delta U)^{n_1} \left(\frac{\nu}{h}\right)^{n_2} \qquad (1)$$

In applying equation (1) to a water brake operating in regime IV, the following assumptions are made:

(1) The surfaces are annular in shape of width d and mean radius r_m (fig. 1).

(2) The annular surfaces rotate relative to one another where ΔU is the difference in tangential velocity between the rotor disk and the water core or between the water core and the housing wall. In other words, the core rotates as a solid body (neglecting the effects of secondary flow and through flow).

(3) The term h is the width of the gradient in tangential velocity between the disk and core or between the core and housing wall, in other words, the thickness of the boundary layer δ (as shown in fig. 2).

(4) Values of 7/4 and 1/4 for the exponents n_1 and n_2, representative of a Blasius type of power law relation, are noted in reference 1 for turbulent flow in smooth pipes and flat plates, and in references 1 and 2 for rotating disks. However, variations from these values will be discussed in the section Effect of Rotative Speed.

By assuming that the force F in equation (1) is concentrated at the mean radius r_m of the core, the torque required to rotate the disk in the housing becomes

$$T = \text{force} \times \text{distance} = 2r_m F \tag{2}$$

or

$$T = C_2 \rho A_w r_m \left(\Delta U_{d-c}\right)^{7/4} \left(\frac{\nu}{\delta_{d-c}}\right)^{1/4} \tag{3}$$

The 2 in equation (2) accounts for the two sides of the disk. Since power is related to torque

$$P = \frac{TN}{C_3} \tag{4}$$

the power absorbed by the disk is

$$P = C_4 \rho A_w N r_m \left(\Delta U_{d-c}\right)^{7/4} \left(\frac{\nu}{\delta_{d-c}}\right)^{1/4} \tag{5}$$

The various dimensionless ratios relating viscous shear to power and torque are noted in appendix B in the terms π_n through π_p. The basic parameter used in the

literature to describe the torque absorbed by a disk rotating in a fluid is the torque coefficient C_m. The relation between torque and torque coefficient is discussed in reference 1, and the remainder of this section is taken in part from reference 1.

The torque or moment absorbed by a disk fully submerged in a fluid (both sides of the disk) is given by the equation

$$T = C_m \frac{\rho \omega^2 a^5}{2g} \tag{6}$$

which is the πa term noted in appendix B. The similarity between equations (6) and (3) becomes apparent if a and a^2 is substituted for the r_m and A_w terms, and if ωa is substituted for the ΔU_{d-c} term in equation (3). The selection of the value for C_m in equation (6) depends on the judgement of existing theoretical and experimental values, which are available in the literature. A general expression for C_m is given by

$$C_m = C_5 (Re)^{-1/5} \tag{7}$$

Values of C_5 range from 0.146 for a free unenclosed disk to 0.0622 for a disk enclosed in a housing when operated at values of Reynolds number high enough to assure a turbulent boundary layer. The lower value more closely resembles the smooth-disk water brake.

Another approach (noted in ref. 2) considers the effect of spacing ratio s/a and uses the expression

$$C_5 = 0.102 \left(\frac{s}{a} \right)^{1/10} \tag{8}$$

For a water brake with a spacing ratio of 0.05, equation (8) results in a value of C_5 of 0.0756.

Equations (6) to (8) apply to a fully submerged smooth disk. However, a water brake does not operate fully submerged, as noted previously. The degree of submergence of the disk in the fluid is accounted for by the submergence ratio X, defined as d/a. The value of X for a fully submerged disk is 1.0, and for an unsubmerged disk is 0. The ratio of the torque absorbed between a partially submerged and fully submerged disk is equal to the ratio of C_m and $C_{m,X=1}$. In other words, for a water brake operating at a given speed over a range of submergence, the torque absorbed varies by the ratio $(C_m/C_{m,X=1})$. This ratio is discussed later in the section Performance Data.

Finally, the increase in pressure radially through the water core due to the centrifugal force of the cores rotation is defined by the equation

$$\frac{\Delta p}{\Delta r} = C_6 \rho \frac{(U_c)^2}{r_m} \tag{9}$$

INTERNAL FLOW ANALYSIS

The existence of a rotating core and a secondary-flow field within the core, noted previously in the discussion of the regime IV flow model, has been substantiated by the flow measurements made on a 46.0-centimeter (18.1-in.) smooth disk rotating fully submerged in air (reported in ref. 2). The results of these flow measurements (fig. 3) show the effect of through flow Q on the radial and circumferential components of the flow velocity (as a ratio of disk speed) and flow direction at two different rotative speeds (proportional to Reynolds number). The figure shows the presence of a rotating core of fluid between the disk and housing wall boundary layers and is the basis for the assumptions used herein in constructing the vector diagram models discussed in the remainder of this section. It is also noted in figure 3 that the flow conditions vary radially within the core. However, a water brake operates partially submerged at a relatively low value of d/a. Therefore, it was assumed that the flow conditions at the mean radius r_m of the water annulus of the water brake adequately represent the flow conditions over the radial extent of the water annulus and core.

Since the core is located between the disk and housing, the core rotates tangentially within the housing at some velocity below that of the disk. The shearing drag forces in the boundary layer are generated by the difference in tangential velocity between the disk, core, and wall. Neglecting the effects of through flow Q, the total shear force between the disk and core must equal the total shear force between the core and housing wall. If no secondary flow Q_s, or through flow Q is present, the mean radius vector diagrams for the flow in the area between the disk and core and between the core and the housing wall are as shown in figures 4(a) and (b), respectively. The values for ΔU_{d-c} and ΔU_{c-w} shown in the diagrams are the magnitude of the gradient in water velocity in the boundary layers causing the shearing action between the disk and core and between the core and housing wall.

The effect of superimposing secondary flow into the flow model is shown by the modification to the vector diagram noted in figure 5. On the disk (fig. 5(a)) the secondary flow vector V_s is directed radially outward (vertically down on the diagram) from the end of the disk vector U_d. This results in an increase in the velocity gradient in

the disk boundary layer ΔV_{d-c} and a change in its direction, tending to skew it radially outward. The same change occurs in the housing wall boundary layer (fig. 5(b)) but in the reverse direction since, as will be shown later, the pressure force created in the core by its tangential rotation around the housing causes the secondary flow to be directed radially inward. Assuming the core vector U_c remains unchanged from its value in figure 4 (a reasonable assumption since the tangential components of the disk and housing wall vectors remained unchanged), the direction of the relative velocity vectors ΔV_{d-c} and ΔV_{c-w} change, and the magnitude of these vectors becomes greater than the corresponding ΔU vectors.

Finally, it is assumed that the effect of superimposing through flow on the flow model can be represented by the further modification to the vector diagram (fig. 6). As water enters the water brake, it flows radially outward until it reaches the core. The water in the core must then give up some of its tangential momentum to accelerate the incoming water up to the core speed. This interchange of momentum between the incoming through flow and the core slows the rotation of the core, which reduces the magnitude of U_c. Also, the through flow adds a component to the vector diagram V_q, which is directed radially outward.

In figure 6 it becomes apparent that the mechanism for deriving work from the through flow is the increase in the disk tangential shearing vector ΔU_{d-c} that the through flow produces. However, because the core is rotating more slowly, the corresponding housing wall shearing vector ΔU_{c-w} becomes smaller than before. The effect then of through flow is to increase the viscous drag force on the disk, while reducing it on the housing wall. Therefore, these two forces are not in balance when through flow is present; the difference being equal to the tangential momentum that is imparted by the through flow to the water brake housing as its tangential velocity is reduced to zero upon discharge from the water brake.

The resulting vector model can be used to describe the means by which the power input to the disk is transmitted from the disk to the core and incoming through flow and then to the housing. Considering first a force balance on the core

Driving forces on core = drag forces on core

the force driving the core is the viscous shearing force transmitted between the disk and the core (eq. (1)). The drag forces on the core are the viscous shearing force exerted by the housing wall on the core (eq. (1) again) plus the tangential momentum imparted by the core to the incoming through flow

$$F = \frac{wt_q U_c}{g} \tag{10}$$

where wt_q is the combined through flow for both sides of the disk. Next, the forces transmitted from the core to the housing consist of the viscous shearing force between the core and the housing wall (eq. (1)), plus the tangential momentum removed from the through flow by the housing as the through flow is discharged from the water brake (eq. (10)).

Therefore, the following equations relating torque to the ΔU_{d-c} and ΔU_{c-w} components of the vector diagrams can be derived from force equations (1) and (10) as follows:

$$T_{d-c} = C_7 \rho r_m A_w \left(\Delta U_{d-c}\right)^{7/4} \left(\frac{\nu}{\delta_{d-c}}\right)^{1/4} \tag{11}$$

$$T_{c-w} = C_7 \rho \left[r_m A_{w,e} \left(\Delta U_{c-w,e}\right)^{7/4} \left(\frac{\nu}{\delta_{c-w,e}}\right)^{1/4} + r_t A_{w,t} \left(\Delta U_{c-w,t}\right)^{7/4} \left(\frac{\nu}{\delta_{c-w,t}}\right)^{1/4} \right] + \left(r_t wt_q U_c\right) \tag{12}$$

where the torque output from the disk T_{d-c}, must equal the torque absorbed by both the housing side wall and tip wall

$$T_{d-c} = T_{c-w} = T_{c-w,e} + T_{c-w,t} + r_t wt_q U_c \tag{13}$$

When no through flow is present, the last term in equations (12) and (13) drops out. It is also apparent in comparing equations (11) and (12) with equation (6) that the constant C_7 includes the term C_m. A modified form of equations (11) and (12) is used in appendix F where the assumption is made that the 1/4 and 7/4 exponents approach values of 0 and 2, respectively, as Reynolds number approaches the levels of the Kleinsorge water brake. A discussion of the effect of Reynolds number on these exponents is noted in the section Effect of Rotative Speed.

PERFORMANCE DATA

The following experimental and experience data, obtained from the literature on smooth disks and from manufacturers and users of smooth-disk water brakes, were used

to determine the accuracy of the vector diagram model constructed in the previous section. Table I shows the important physical aspects of the reference smooth disks and water brakes used.

Kleinsorge. - In figure 7 are a series of multidisk water brake maximum power curves (maximum partial submergence of the disk in water) and a part-power curve given to the author by Mr. Walter Kleinsorge (now deceased), a German manufacturer of water brakes. Also noted in the figure are the values of water through flow rate and water pressure measured at the tip diameter of his 111-centimeter (43.7-in.) diameter smooth-disk water brake. Note the straight line characteristic of these curves on the log plot. The slopes of the curves indicate that the power absorbed is proportional to the rotative speed to the 2.7 power or

$$P = C_8(N)^{2.7} \tag{14}$$

Daily and Asbedian (ref. 2). - The air data published in this reference and noted previously in figure 3 consists of measured flow angles and velocities. The report also develops a relation between core rotational speed and boundary-layer thickness. This relation is shown plotted in figure 8 and is discussed in the section Effective of Rotative Speed. The water data plotted in figures 9 to 11 show the effect of through flow Q, disk rotational speed ω (which is proportional to Reynolds number), and spacing ratio s/a on torque coefficient C_m for a 46.0-centimeter (18.1-in.) diameter fully submerged disk. The constant in the equation noted in figure 10

$$C_m = \frac{0.0793}{(Re)^{1/5}} \tag{15}$$

was developed by Daily for a spacing ratio s/a of 0.08. The equation is a combination of equations (7) and (8) where it was assumed that the standard boundary-layer power law would be proportional to $Re^{-1/5}$ (turbulent flow). The increase in C_m with through flow noted in figure 10 is explained by the increase that was obtained in the U_{d-c} vector when the effect of through flow was added between the vector diagrams of figures 5(a) and 6(a). This effect is discussed in the section Effect of Through Flow.

Watabe (ref. 3). - Figures 10 and 12 show the effect of disk rotational speed ω (proportional to Reynolds number) on the torque coefficient of a fully submerged 22.6-centimeter (8.9-in.) diameter disk. No through flow was used. A broad enough range of Re was covered to establish the fact that the disk operated in a turbulent flow regime above $Re = 1 \times 10^6$. This is shown in figure 10.

Test data are also shown for a configuration having standing circumferential rings (grooves) attached to one side of the disk and housing wall. This is shown schematically

in figure 12(a). The presence of the grooves would prevent the formation of secondary flows in the core, and thus helped to determine the magnitude and effect of these flows on performance.

The effect of the grooves on performance is shown in figure 12(b). Adding the grooves to the disk decreased the torque coefficient C_m, which may be explained by referring to the vector diagram of figure 5(a). The presence of grooves on the disk would increase the ratio of disk-to-housing wall surface area in contact with the core, increasing U_c and thereby decreasing ΔU_{d-c} and C_m. Adding grooves to both the disk and housing restored the ratio of the disk to housing wall surface area and increased ΔU_{d-c} and C_m to their original values without grooves.

Also, as noted previously, the presence of the grooves on the disk and housing walls would tend to reduce or eliminate the magnitude of the secondary flow in the core and thus help to determine its effect on performance. The vector diagrams of figures 5 and 6 provide for no effect of secondary flow V_s, on ΔU_{d-c}. This effect is substantiated in figure 12(b) where the close agreement in C_m between the two upper curves of data from reference 3 indicate the independence between the secondary flow V_s, the velocity gradient in the disk boundary layer ΔU_{d-c}, and the core rotational speed U_c.

Deavers (ref. 4). - The data from this reference, obtained on a fully submerged 14.0-centimeter (5.5-in.) smooth disk with an unspecified amount of water through flow, are shown plotted with the Kleinsorge curves in figure 7. These data are also shown plotted in figures 12 and 14 in terms of C_m and will be discussed later.

Ketola and McGrew (ref. 5). - The result of this analysis is a prediction of the effects of partial submergence on core rotational velocity ratio k_o and torque coefficient C_m. The result, for a level of Re and spacing ratio s/a high enough to be in the turbulent flow regime IV, is plotted in figure 13.

Wosika (ref. 6). - The experimental data on a 20.3-centimeter (8.0-in.) smooth-disk water brake reported in this reference were used to validate the effect of partial disk submergence on power absorption (as predicted in ref. 5). The very close correlation between the predicted curve of reference 5 and the data of reference 6 is shown in figure 13(a).

COMPARISON OF FLOW MODEL WITH DATA

In this section, the effects of water through flow, secondary flow, and disk and core rotational speed, assumed in the vector analysis of the section INTERNAL FLOW ANALYSIS, are compared with the data of figures 3 and 9 to 12 to determine the validity of the model. The numerical examples used to make the comparisons are given in appendixes C to F.

Effect of Through Flow

The exact effect of through flow on performance is not clear. On first examination of figure 9(a), C_m appears to be a linear function of Q over the lower range of through flows considered. For values of Q from 0 to 0.0017 cubic meters per second (0 to 0.06 ft^3/sec), the equation for the straight line portion of the curve shown is

$$C_m = C_g + \left(\frac{\Delta C_m}{\Delta Q_q}\right) Q$$

$$= 0.00427 + 0.83Q \qquad \text{in SI units or}$$

$$= 0.00427 + 0.023Q \qquad \text{in U.S. customary units} \tag{16}$$

At higher values of Q, the increase in C_m with Q approached zero. However, after further inspection, it appears that the effect of through flow on torque coefficient could be exponential. This is apparent in figure 9(b), which is figure 9(a) replotted on log-log scales from which the following equation was constructed:

$$C_m = 0.014(Q)^{1/7} \quad \text{or}$$

$$= 0.0084(Q)^{1/7} \tag{17}$$

Therefore, either equation (16) or (17) may correctly represent the effect of Q on C_m over the range of Q considered.

Nevertheless, the vector diagrams were constructed at two points along the curve of figure 9(a) for the smooth disk of reference 2: one point at zero through flow and the other at a value of through flow Q of 0.0028 cubic meters per second (0.1 ft^3/sec). This was done to determine the validity of the through-flow effects assumed in the vector diagrams of figure 6. The calculations for the vector diagrams for these two points are noted in appendix C. The resulting mean-radius vector diagrams are shown in figure 15. From these diagrams it is apparent that the tangential velocity gradient (shearing force in the tangential direction) between the disk and core increases with through flow by the ratio

$$\left(\frac{\Delta U}{\Delta U_{Q=0}}\right)_{d-c} = \frac{6.0}{4.4} = 1.37$$

From figure 9(a) it is apparent that the torque coefficient also increases by approximately the same amount

$$\frac{C_m}{C_{m,Q=0}} = \frac{0.00604}{0.00427} = 1.41$$

Therefore, from this agreement between the tangential shearing force and the torque coefficient it appears that C_m and ΔU_{d-c} increase proportionally with the addition of through flow. Thus, the effect of through flow assumed in the construction of the vector diagram model of figure 6 agrees with the data of reference 2.

Effect of Rotative Speed

The data of figures 3 and 11 were reduced to vector quantities to determine the validity of the disk and core rotational speed effects assumed in the vector diagram models of figures 4 and 5. Two rotative speeds (two Reynolds numbers) were considered with through flow. The calculations for the vector diagrams are noted in appendix D. The through-flow value used was 0.0025 cubic meter per second (0.089 ft^3/sec). The two values of Reynolds number used (for water) were 2.9×10^6 and 6.9×10^6, both in the turbulent flow regime. These two values of Re were intentionally made greater, by a factor of 10, than the air data of figure 3 in order to fairly compare the air data with the water data of figure 11. This interpretation was felt to be justified because the transition from laminar to turbulent flow was observed in reference 2 to differ between air and water by a factor of approximately 10.

The resultant vector diagrams are shown in figure 16. From them, the ratio of ΔU_{d-c} at high and low rotative speed is noted to be

$$\left(\frac{\Delta U_{d-c,\,high\ Re}}{\Delta U_{d-c,\,low\ Re}}\right) = \left(\frac{38}{18.5}\right) = 2.05$$

In equation (5), power absorption is proportional to the disk rotative speed times the velocity gradient between the disk and core to the 7/4 power, or $U_d\left(\Delta U_{d-c}\right)^{7/4}$ in terms of vector quantities. However, the width of the velocity gradient (boundary-layer thickness δ) also effects power absorption. This is seen in equation (5) as $\delta^{-1/4}$. Therefore, the following ratios for the power absorbed at high and low rotative speeds (high and low Reynolds number) can be written as

$$\left(\frac{P_{\text{high Re}}}{P_{\text{low Re}}}\right) = \frac{\left[\text{Re}\left(\Delta U_{d-c}\right)^{7/4}\,\delta^{-1/4}\right]_{\text{high Re}}}{\left[\text{Re}\left(\Delta U_{d-c}\right)^{7/4}\,\delta^{-1/4}\right]_{\text{low Re}}} \tag{18}$$

Both the rotative speed of the disk (Reynolds number) and the rotative speed of the core ($U_d k_o$), which is effected by through flow, have been found to effect the thickness of the boundary layer. These effects are shown in figure 8, which is a plot of air data obtained from figure 41 of reference 2. Figure 8 shows that the value of $\left[\delta(\text{Re})^{1/5}/r\right]$ decreases from 0.22 to 0.165 between $\text{Re} = 2.9\times10^5$ and 6.9×10^5, which indicates a 37-percent decrease in δ at a given radius r. Substituting these values into equation (18), the calculated ratio of power between the two speeds is

$$\frac{P_{\text{high Re}}}{P_{\text{low Re}}} = \left(\frac{6.9}{2.9}\right)(2.05)^{7/4}(0.63)^{-1/4} = 9.4$$

By comparison, equation (6) for torque (the π_a relation in appendix B) can be combined with equation (4) for power and written as

$$\frac{P_{\text{high Re}}}{P_{\text{low Re}}} = \frac{(TN)_{\text{high Re}}}{(TN)_{\text{low Re}}} = \frac{\left(C_m\omega^2 N\right)_{\text{high Re}}}{\left(C_m\omega^2 N\right)_{\text{low Re}}} = \frac{C_m(\text{Re})^3_{\text{high Re}}}{C_m(\text{Re})^3_{\text{low Re}}} = 13.4\,\frac{\left(C_m\right)_{\text{high Re}}}{\left(C_m\right)_{\text{low Re}}} \tag{19}$$

Obtaining the value for the ratios of C_m from figure 11 at $s/a = 0.069$, the measured ratio of power between the two speeds is

$$\frac{P_{\text{high Re}}}{P_{\text{low Re}}} = 13.4 \times 0.76 = 10.2$$

which agrees within 8 percent of the value of 9.4 obtained previously by using the Blasius power law (eq. (5)) and the velocity diagram relation of figure 16.

The agreement, however, may be closer than 8 percent. The Blasius power law applies only to the case where the velocity distribution in the boundary layer varies with the 1/7 power of the distance through the boundary layer.

$$\frac{U}{U_c} = \left(\frac{s}{\delta}\right)^{1/\eta} \tag{20}$$

It is noted in reference 1 that the exponent in this equation varies with Reynolds number from 1/6 for flows that are barely turbulent to 1/10 at higher Reynolds numbers. These results were obtained from pipe flow experiments which, according to the reference, are valid for flow over flat plates and rotating disks. The boundary-layer measurements made in air in reference 2 indicated close agreement with a value of 1/7. The particular measurements were made at zero through flow and $Re = 6.9 \times 10^5$. When run over a range of Reynolds numbers from 1.6×10^6 to 6.9×10^6 (fig. 51 in ref. 2 and fig. 10 herein) at zero through flow, the result was a variation in C_m characteristic of the turbulent side of the transition region. With a through flow of 0.0025 cubic meter per second (0.089 ft^3/sec), however, a fully turbulent flow regime well beyond the transition region was indicated (fig. 10). Therefore, it is reasonable to assume that an exponent of less than 1/7 would represent the velocity distribution in the boundary layer. Figure 20.3 of reference 1 indicates a rapid decrease in the value of this exponent with increasing turbulence. The reference indicates that a value of, for instance, 1/9, results in a corresponding change in the n_1 and n_2 exponents in the Blasius power law (eq. (5)) to 11/6 and -1/6, respectively. The resulting value for equation (18) would then be

$$\frac{P_{\text{high Re}}}{P_{\text{low Re}}} = \left(\frac{6.9}{2.9}\right)(2.05)^{11/6}(0\ 63)^{-1/6} = 9.6$$

which agrees within 6 percent of the measured power ratio between these two speeds of 10.2.

In either case, these power ratios represent relatively close agreement between the performance derived from the vector diagrams (derived with the aid of fig. 3 and the Blasius power equation) and the measured performance using the data of figures 8 and 11. The vector diagram model, therefore, appears to account for the effects of speed changes reasonably well between the two speeds investigated.

Example Operating Point For Kleinsorge Water Brake

The torque coefficient and Reynolds number were determined at two known operating points for the 111-centimeter (43.7-in.) smooth-disk Kleinsorge water brake. One point was where the water through-flow rate was known, and the other point was where the water pressure at the outer radius a of the water annulus was known. The calculation

of these values is noted in appendix E. The two points are plotted in figure 14 along with a replot of the C_m against Re curves of references 2 to 4 shown in figures 10 and 12(b) and extrapolated to the higher values of Re where the Kleinsorge operating points are located. The close agreement between the Kleinsorge operating points and the curves of reference 2 (Daily) are coincidental. The points are for partially submerged operation with through flow, and the curves are for fully submerged operation without through flow. These differences may have been counterbalancing. The extension of Deavers data (ref. 4) with through flow resulted in a curve that is somewhat higher than the Kleinsorge operating points. The model for the Watabe smooth-disk data (ref. 3) was similar to Daily's, but the resulting torque coefficient curve was lower. However, in spite of the mismatch, it is assumed that the slope of the curves (fig. 14) are representative of the variation of C_m with Re at a given water depth d for the Kleinsorge water brake.

Because the Kleinsorge water brake operates with its disk partially submerged, the data of references 5 and 6 (fig. 13) was used to determine the amount of submergence. From this submergence and from the known water pressure at the tip radius of the housing, the core rotational speed was computed and compared with the data of reference 2. The data in figure 13 is for zero through flow. Therefore, the effects of through flow were accounted for by comparing the tangential shearing vectors of the vector diagrams, as was done previously in the section Effects of Through Flow. The analysis, including the development of the disk vector diagram at the 4700 rpm operating point, is noted in appendix F.

The resultant disk vector diagram, which includes the effect of through flow and secondary flow, is shown in figure 17(a). The vector values noted are at the mean radius of the water annulus. The resultant water depth d, computed to be 5.28 centimeters (2.08 in.) in appendix F, falls between the value Kleinsorge assumed (2.54 cm; 1 in.) and what the industrial users of the water brake have observed (6.1 to 8.1 cm; 2.4 to 3.2 in.). A water depth of 5.28 centimeters (2.08 in.) would indicate that only 9.5 percent of the disk radius is submerged in water. Values of k_o (the ratio of the core to disk rotational speed) of between 0.404, computed for a water depth of 5.28 centimeters (2.08 in.) and a housing water pressure of 141 newtons per square centimeter (205 lb/in.^{2}), and 0.385, computed from the vector diagrams, agree well with the values of k_o noted in figure 3(b) for the lowest through-flow rate.

The resulting vector diagram for the housing wall, corresponding to the vector diagram just noted for the disk side of the core, is shown in figure 17(b). The secondary flow vector V_s was made equal but opposite in direction to its value on the disk side of the core reflecting the continuity of flow that was assumed in the secondary flow path (fig. 2). It may be noted that the resulting skew angle of -15^o almost exactly matches the flow angle measured in the wall boundary layer at low through-flow rates for the

smooth disk of figure 3(b). It may also be noted in figures 17(a) and (b) that the resultant ratio of radial through-flow vector to disk speed, $V_q/U_d = 0.2/260 = 0.001$, is negligibly small. In figure 3(b) the corresponding values of V_r/U_d corrected to the hub, mean, and tip locations noted in the figure indicated that the curves for the lowest through-flow rate shown are the most representative of the operation of the water brake.

The effect of through flow on the vector diagrams may be noted by comparing the diagrams of figure 17(a) with 17(c). The effect is a 10-percent reduction in the core rotational velocity U_c and a corresponding 8-percent increase in the disk-to-core tangential shearing vector ΔU_{d-c}. However, the flow skew angle on the disk remains essentially unchanged from 9^o radially outward with through flow to 10^o without through flow. It is also observed from figure 17(c) and from the discussion of equations (11) and (12) in appendix F, that without through flow the torque transmitted from the disk to the core agrees within 5 percent of the torque transmitted from the core to the housing walls, with 60 percent of the torque transmitted to the housing side wall and the remaining 40 percent to the housing tip wall.

SUMMARY OF RESULTS

A method of describing the power absorption and internal flow characteristics of a smooth-disk water brake through the development of vector diagrams has been presented. The results may be summarized as follows:

1. Housing wall and disk vector diagrams were constructed for a reference 46.0-centimeter (18.1-in.) smooth disk operating fully submerged in air and in water, where the effects of core rotation, through flow, and secondary flow were considered. The measured changes in power absorption with changes in through flow and rotational speed agreed closely with the changes predicted in the disk shearing force calculated from the vector diagram model and from a modified form of the Blasius power law.

2. Comparable housing wall and disk vector diagrams were constructed for a 111-centimeter (43.7-in.) smooth-disk water brake (disk partially submerged in water), based on its known operating characteristics at one value of through flow, and for zero through flow. Using the vector diagrams, close agreement (within 5 percent) was obtained between the calculated torque transmitted from the disk to the core, and from the core to the housing walls, indicating the validity of the flow model and the vector diagram representation of the water brake.

3. The amount of disk submergence for the 111-centimeter (43.7-in.) water brake, computed with the aid of the vector diagram model, a known water pressure, and data from a reference 20.3-centimeter (8.0-in.) water brake was 5.28 centimeters (2.08 in.), or 9.5 percent of the disk radius, which agreed reasonably well with operational experience.

4. The analysis of the vector diagrams, calculated for the 111-centimeter (43.7-in.) diameter Kleinsorge water brake indicated the following: (a) The core rotated at approximately 40 percent of disk speed. (b) The secondary flow in the core had no effect on the torque absorbed, but skewed the flow radially inward on the housing wall by approximately 15° and radially outward on the disk by approximately 9°. (c) The through flow increased the torque absorbed by approximately 8 percent but had little effect on the direction of flow on the disk or housing wall. (d) Sixty percent of the torque transmitted to the housing walls due to the viscous shearing of water between the core and housing was through the housing end wall, and the remaining 40 percent was through the housing tip wall.

Lewis Research Center,
National Aeronautics and Space Administration,
Cleveland, Ohio, January 24, 1973,
501-24.

APPENDIX A

SYMBOLS

The F, T, and L dimensions are noted for the terms used in the dimensional analysis of appendix B, where F is force, L is length, and T is time. The dimension F is also used for mass for convenience. The four quantities are dimensionally equivalent; that is, the dimensions of mass M are FT^2L^{-1}

A	area, cm^2 (ft^2); L^2
a	tip radius of disk or housing, cm (ft); L
C_1, C_2, etc.	exponents on primary quantities in appendix B; constants of proportionality and unit conversions everywhere else
C_m	torque coefficient; π_a term
D	drag, N (lb); F
d	water depth, cm (in.); L
e	fluid bulk modulus, N/cm^2 (lb/ft^2); FL^{-2}
F	force, N (lb); F
g	unit conversion or gravity, $m\text{-}kg/sec^2N$ (ft/sec^2); LT^{-2}
h	width of velocity gradient (see eq (1)), cm (in.); L
k	ratio of $U_c/\omega a$ or U_c/U_d; π_f term
k_o	ratio of $U_c/\omega a$ or U_c/U_d midway between disk and housing wall
N	rotative speed, rpm; T^{-1}
n_1, n_2, etc.	exponents
P	power, kW (hp); FLT^{-1}
p	absolute pressure, N/cm^2 (lb/ft^2), except where noted; FL^{-2}
Q	volume flow or through-flow rate wt/ρ, m^3/sec (ft^3/sec); L^3T^{-1}
$\overline{Q}$	source flow number (ref. 2); π_e term
Re	Reynolds number $\omega a^2/\nu$; π_c term
r	radius, cm (in.); L
s	axial spacing or axial distance from the disk, cm (in.); L
T	torque, mN (ft lb); LF

$\mathcal{T}$	through-flow number (ref. 2); π_d term
U	tangential velocity, m/sec (ft/sec); LT^{-1}
V	through-flow, resultant, or radial velocity, m/sec (ft/sec); LT^{-1}
W	work, MN (ft lb); FL
wt	weight flow rate, kg/sec (lb/sec); FT^{-1}
X	depth of water annulus ratio or submergence ratio, d/a; π_j term
α	angle from tangential direction, deg
δ	boundary-layer thickness, cm (in.); L
λ	undefined length, cm (ft); L
μ	dynamic viscosity, kg sec/cm^2 (lb sec/ft^2); FTL^{-2}
ν	kinematic viscosity μ/ρ, cm^2/sec (ft^2/sec); L^2T^{-1}
ρ	fluid mass density, kg sec^2/cm^4 (lb sec^2/ft^4); FT^2L^{-4}
σ	surface tension, N/cm (lb/ft); FL^{-1}
τ	shear stress of fluid, N/cm^2 (lb/ft^2); FL^{-2}
ω	disk angular velocity, rad/sec; T^{-1}

Subscripts:

c	center (core) region of water annulus
D	Daily
d	disk
e	end (side) wall of housing
eff	effective
h	hub radius of water annulus
k	Kleinsorge
m	mean radius of water annulus
q	through flow or due to through flow
r	radial
s	secondary flow or due to secondary flow
t	tip or tip radius of housing, disk, or water annulus
w	wetted or wall

APPENDIX B

DIMENSIONAL ANALYSIS

Pursuant to developing a general flow model describing the internal flow behavior and overall performance of a smooth disk water brake, a dimensional analysis was made to develop the parameters that could relate each of the internal flow regimes and performance characteristics to the viscous shear term τ. The resulting prediction equation is made up of independent dimensionless parameters (pi terms), which are analyzed and compared with the equations and data from the water brake performance curves of Kleinsorge and the various other references noted herein.

The pertinent quantities are assumed to be

$$\tau = f(\rho, \nu, \Delta U, a, \lambda, \omega, D, T, g, A, \sigma, e, Q, \Delta p, p, V, P)$$

or in equation form

$$C_\tau{}^{C1}{}_\rho{}^{C2}{}_\nu{}^{C3}{}_{\Delta U}{}^{C4}{}_a{}^{C5}{}_\lambda{}^{C6}{}_\omega{}^{C7}{}_D{}^{C8}{}_T{}^{C9}{}_g{}^{C10}{}_A{}^{C11}{}_\sigma{}^{C12}{}_e{}^{C13}{}_Q{}^{C14}{}_{\Delta p}{}^{C15}{}_p{}^{C16}{}_V{}^{C17}{}_P{}^{C18} = 0$$

having the following dimensions:

$$\overset{\tau}{(FL^{-2})}^{C1}\overset{\rho}{(FT^2L^{-4})}^{C2}\overset{\nu}{(L^2T^{-1})}^{C3}\overset{\Delta U}{(LT^{-1})}^{C4}\overset{a}{(L)}^{C5}\overset{\lambda}{(L)}^{C6}\overset{\omega}{(T^{-1})}^{C7}$$

$$\times\overset{D}{(F)}^{C8}\overset{T}{(FL)}^{C9}\overset{g}{(LT^{-2})}^{C10}\overset{A}{(L^2)}^{C11}\overset{\sigma}{(FL^{-1})}^{C12}\overset{e}{(FL^{-2})}^{C13}\overset{Q}{(L^3T^{-1})}^{C14}$$

$$\times\overset{\Delta p}{(FL^{-2})}^{C15}\overset{p}{(FL^{-2})}^{C16}\overset{V}{(LT^{-1})}^{C17}\overset{P}{(LFT^{-1})}^{C18} = F^oT^oL^o$$

where according to Buckingham's pi Theorem, with 18 quantities and three dimensions, there would be 15 pi terms.

The resulting 15 pi terms are developed and listed in table II. Through a rearrangement of these 15 basic pi terms, the following pi terms, which are consistent with those noted in references 1 to 5, were obtained:

$$\pi_a = \frac{\pi_5}{\pi_7^2 \pi_2} = \frac{Q^2}{\omega^2 a^6} \frac{a^2 D}{\rho Q^2} \frac{T}{aD} = \frac{T}{\rho \omega^2 a^5} \text{ (Torque coefficient, } C_m)$$

$$\pi_b = \frac{\pi_{12}}{\pi_2 \pi_4^2 \pi_{13}^2} = \frac{\Delta p a^2}{D} \frac{Q^2}{\Delta U^2 a^4} \frac{a^2 D}{\rho Q^2} \frac{\Delta U^2}{U_c^2} = \frac{\Delta p}{\rho U_c^2} \text{ (Water pressure in housing)}$$

$$\pi_c = \frac{\pi_7}{\pi_3} = \frac{\omega a^3}{Q} \frac{Q}{\nu a} = \frac{\omega a^2}{\nu} \text{ (Reynolds number)}$$

$$\pi_d = \frac{(\pi_c)^{1/5}}{\pi_7} = \frac{Q}{\omega a^3} \left(\frac{\omega a^2}{\nu}\right)^{1/5} \text{ (Through flow number, } \mathcal{F})$$

$$\pi_e = \frac{1}{\pi_6 \pi_7} = \frac{Q}{\omega a^3} \frac{a}{s} = \frac{Q}{s a^2 \omega} \text{ (Source flow number, } \overline{Q})$$

$$\pi_f = \frac{\pi_4 \pi_{13}}{\pi_7} = \frac{\Delta U a^2}{Q} \frac{U_c}{\Delta U} \frac{Q}{\omega a^3} = \frac{U_c}{\omega a} \text{ (k or } k_o)$$

$$\pi_g = \frac{\pi_5}{\pi_2 \pi_7} = \frac{T}{aD} \frac{a^2 D}{\rho Q^2} \frac{Q}{\omega a^3} = \frac{T}{\rho Q \omega a^2} \text{ (Effect of through flow on T)}$$

$$r_h = f(\pi_6) = \frac{\lambda}{a} \times \frac{s}{\lambda} = \frac{s}{a} \text{ (Similarity in geometry)}$$

$$\pi_i = \frac{1}{\pi_7} = \frac{Q}{\omega a^3} \text{ (Disk boundary layer, through flow, or secondary flow term)}$$

$$\pi_j = f(\pi_6) = \frac{d}{a} \text{ (Depth of water ratio, X)}$$

The following additional pi terms were also obtained. They were not used in the references, but may influence the process, and should be considered when modeling or describing the problem:

$$\pi_k = \frac{\pi_2 \pi_4^2 \pi_{13}^2}{\pi_{11}} = \frac{D}{ea^2} \frac{\rho Q^2}{a^2 D} \frac{\Delta U^2 a^4}{Q^2} \frac{U^2}{\Delta U^2} = \frac{\rho U_d^2}{e} \text{ or } \frac{\rho U_c^2}{e} \text{ (Cauchy number or Mach number effect)}$$

$$\pi_l = \frac{\pi_2 \pi_4^2 \pi_{13}^2}{\pi_{10}} = \frac{D}{a\sigma} \frac{\rho Q^2}{a^2 D} \frac{\Delta U^2 a^4}{Q^2} \frac{U^2}{\Delta U^2} = \frac{\rho a U^2}{\sigma} \text{ (Weber number or surface tension effect)}$$

$$\pi_m = \frac{\pi_{13}^2 \pi_4^2}{\pi_8} = \frac{\Delta U^2 a^4}{Q^2} \frac{Q^2}{a^5 g} \frac{U^2}{\Delta U^2} = \frac{U^2}{ag} \text{ (Froule number or gravity effects)}$$

$$\pi_n = \frac{\pi_1 \pi_9}{\pi_5} = \frac{\tau a^2}{D} \frac{aD}{T} \frac{A}{a^2} = \frac{\tau A a}{T} \text{ (Viscous shear)}$$

$$\pi_o = \frac{1}{\pi_2 \pi_4^2 \pi_9} = \frac{a^2 D}{\rho Q^2} \frac{Q^2}{\Delta U^2 a^4} \frac{a^2}{A} = \frac{D}{\rho \Delta U_{d-c}^2 A} \text{ (Surface drag)}$$

$$\pi_p = \frac{\pi_{15}}{\pi_7 \pi_1} = \frac{Pa^2}{QD} \frac{Q}{\omega a^3} \frac{D}{\tau a^2} = \frac{P}{\omega a^3 \tau} \text{ (Power parameter)}$$

$$\pi_r = \frac{\pi_1}{\pi_2 \pi_3 \pi_6 \pi_7} = \frac{\tau a^2}{D} \frac{Q}{\nu a} \frac{Q}{\omega a^3} \frac{a^2 D}{\rho Q^2} \frac{s}{a} = \frac{\tau s}{\nu \rho \omega a} \text{ (Viscous shear stress)}$$

$$\pi_s = \pi_a \pi_7 \pi_9 = C_m \frac{\omega a^3}{Q} \frac{A}{a^2} = \frac{C_m \omega a A}{Q} \text{ (T against Q)}$$

Rewriting the equation in terms of the resulting pi terms

$$\pi_r = f(\pi_a, \pi_b, \ldots)$$

results in a prediction equation for τ as follows:

$$\tau = \frac{\nu \rho \omega a}{s} f\left(C_m, \frac{\Delta p}{\rho U_c^2}, \text{Re}, \mathscr{F}, \bar{Q}, k_o, \frac{T}{\rho Q \omega a^2}, \frac{s}{a}, \frac{Q}{\omega a^3}, X, \frac{\rho U^2}{e}, \frac{\rho a U^2}{\sigma}, \frac{U^2}{ag}, \frac{D}{\rho \Delta U^2 A}, \right.$$

$$\left. \frac{\lambda}{s}, \frac{V}{\Delta V}, \frac{\Delta p}{p}, \text{etc.} \right)$$

APPENDIX C

SAMPLE PROBLEM: EFFECT OF THROUGH FLOW

This numerical example was derived to determine the effects of water through flow on the vector diagrams for the smooth disk of reference 2, using the air data of figure 3(a) as the flow model.

$$a = 23.0 \text{ cm} \quad \text{or} \quad 9.06 \text{ in.}$$

$$\frac{s}{a} = 0.069$$

from table I.

$$\frac{r_m}{a} = 0.65$$

which is the mean radius ratio (see fig. 3).

$$Q_q = 0 \text{ and } 0.00283 \text{ m}^3/\text{sec} \quad \text{or} \quad 0.10 \text{ ft}^3/\text{sec}$$

from figure 9(a).

$$Re_{water} = 2.4 \times 10^6$$

$$Re_{air} = 2.9 \times 10^5$$

for just barely turbulent flow. The factor of 10 difference in Re between the two fluids was used because the transition to turbulent flow was observed to differ by a factor of approximately 10 in the reference.

$$\frac{s_{eff}}{s} = 0.75$$

which is the assumed effect of boundary-layer displacement thickness for just barely turbulent flow in air (fig. 3(a)).

$$s_{eff} = \left(\frac{s}{a}\right) \times a \times \left(\frac{s_{eff}}{s}\right)$$

$$= 0.069 \times 23.0 \times 0.75 = 1.19 \text{ cm}$$

$$= 0.069 \times 9.06 \times 0.75 = 0.47 \text{ in.}$$

$$r_m = \left(\frac{r_m}{a}\right) \times a$$

$$= 0.65 \times 23.0 = 15.0 \text{ cm}$$

$$= 0.65 \times 9.06 = 5.90 \text{ in.}$$

$$A_q = 2 \times 2\pi r \times s_{eff}$$

$$= 4\pi \times 15.0 \times 1.19 = 225 \text{ cm}^2$$

$$= 4\pi \times 5.90 \times 0.47 = 35 \text{ in.}^2$$

where A_q is the cross section perpendicular to the through flow at radius r_m.

$$V_q = \left(\frac{Q}{A}\right)_q$$

$$= \frac{0.00283}{225} \times 10^4 = 0.126 \text{ m/sec}$$

$$= \frac{0.10}{35} \times 144 = 0.411 \text{ ft/sec}$$

$$\omega a = \frac{Re_{water}\ \nu}{a}$$

$$= \frac{2.4\times10^{6} \times 0.984 \times 10^{2}}{1\times10^{6} \times 23.0} = 10.3 \text{ m/sec}$$

$$= \frac{2.4\times10^{6} \times 10.6 \times 12}{1\times10^{6} \times 9.06} = 34 \text{ ft/sec}$$

$$\omega r_m = \omega a \times \left(\frac{r_m}{a}\right)$$

$$= 10.3 \times 0.65 = 6.7 \text{ m/sec}$$

$$= 34 \times 0.65 = 22 \text{ ft/sec}$$

$$\left(\frac{V_q}{\omega r_m}\right) = \frac{0.126}{6.7} = 0.019$$

$$k_o = \frac{U_c}{\omega r_m}$$

$$= 0.34 \quad (Q = 0)$$

$$= 0.10 \quad (\text{with } Q)$$

from figure 3(a).

$$U_c = \frac{U_c}{\omega r_m} \times \omega r_m$$

$$\left.\begin{aligned} &= 0.34 \times 6.7 = 2.3 \text{ m/sec} \\ &= 0.34 \times 22 = 7.5 \text{ ft/sec} \end{aligned}\right\} \quad Q = 0$$

$$\left.\begin{aligned} &= 0.10 \times 6.7 = 0.7 \text{ m/sec} \\ &= 0.10 \times 22 = 2.2 \text{ ft/sec} \end{aligned}\right\} \quad \text{with } Q$$

$$\Delta U_{d\text{-}c} = \omega r_m - U_c$$

$$\left.\begin{aligned} &= 6.7 - 2.3 = 4.4 \text{ m/sec} \\ &= 22 - 7.5 = 14.5 \text{ ft/sec} \end{aligned}\right\} \quad Q = 0$$

$$\left.\begin{aligned} &= 6.7 - 0.7 = 6 \text{ m/sec} \\ &= 22 - 2.2 = \sim 20 \text{ ft/sec} \end{aligned}\right\} \quad \text{with } Q$$

The resulting vector diagrams are noted in figure 15 and discussed in the section Effect of Through Flow.

APPENDIX D

SAMPLE PROBLEM: EFFECT OF ROTATIVE SPEED

This numerical example was used to determine the vector diagram characteristics of the reference 2 smooth disk at two different speeds with through flow.

$$a = 23.0 \text{ cm}$$

$$= 9.06 \text{ in.}$$

$$\frac{s}{a} = 0.069$$

from table I.

$$\frac{r_m}{a} = 0.65$$

where r_m/a is the radius ratio at which vector diagrams are determined.

$$Q_{q,\,water} = 0.0025 \text{ m}^3/\text{sec}$$

$$= 0.089 \text{ ft}^3/\text{sec}$$

$$Re_{air} = 2.9\times10^5 \text{ and } 6.9\times10^5$$

from figures 3(a) and (b).

$$Re_{water} = 2.9\times10^6 \text{ and } 6.9\times10^6$$

The factor of 10 difference in Re between the two fluids was used because the transition to turbulent flow was observed to differ by approximately a factor of 10 in the reference.

$$\frac{s_{eff}}{s} = 0.75$$

from appendix C.

$$\omega r_m = \frac{Re_{water}\ \nu}{a} \times \frac{r_m}{a}$$

$$= \frac{\left|\begin{matrix}2.9\\6.9\end{matrix}\right| \times 10^6 \times 0.984 \times 10^2 \times 0.65}{1 \times 10^6 \times 23.0} = \left|\begin{matrix}8.1\\19.2\end{matrix}\right| \text{ m/sec}$$

$$= \frac{\left|\begin{matrix}2.9\\6.9\end{matrix}\right| \times 10^6 \times 10.6 \times 12 \times 0.65}{1 \times 10^6 \times 9.06} = \left|\begin{matrix}26.5\\63.0\end{matrix}\right| \text{ ft/sec}$$

$$V_q = \left(\frac{Q}{A}\right)_q = \frac{0.0025}{225} \times 10^4 = 0.112 \text{ m/sec}$$

$$= \frac{0.089}{35} \times 144 = 0.365 \text{ ft/sec}$$

$$\frac{V_q}{\omega r_m} = \frac{0.112}{\left|\begin{matrix}8.1\\19.2\end{matrix}\right|} = \left|\begin{matrix}0.014\\0.006\end{matrix}\right|$$

$$k_o = \frac{U_c}{\omega r_m} = \left|\begin{matrix}0.30\\0.40\end{matrix}\right|$$

The values 0.30 (fig. 3(a)) and 0.40 (fig. 3(b)) are averages at the mean radius between 0 and the lowest through-flow value shown.

$$U_c = \frac{U_c}{\omega r_m} \times \omega r_m$$

$$= \begin{vmatrix} 0.30 \\ \\ 0.40 \end{vmatrix} \times \begin{vmatrix} 8.1 \\ \\ 19.2 \end{vmatrix} = \begin{vmatrix} 2.4 \\ \\ 7.7 \end{vmatrix} \text{ m/sec}$$

$$= \begin{vmatrix} 0.30 \\ \\ 0.40 \end{vmatrix} \times \begin{vmatrix} 26.5 \\ \\ 63.0 \end{vmatrix} = \begin{vmatrix} 8.0 \\ \\ 25.0 \end{vmatrix} \text{ ft/sec}$$

$$\frac{V_s}{\omega r_m} = \begin{vmatrix} 0.20 \\ \\ 0.12 \end{vmatrix}$$

from figure 3, interpolated between 0 and the lowest through-flow value shown.

$$V_s = \frac{V_s}{\omega r_m} \times \omega r_m$$

$$= \begin{vmatrix} 0.20 \\ \\ 0.12 \end{vmatrix} \times \begin{vmatrix} 8.1 \\ \\ 19.2 \end{vmatrix} = \begin{vmatrix} 1.6 \\ \\ 2.3 \end{vmatrix} \text{ m/sec}$$

$$= \begin{vmatrix} 0.20 \\ \\ 0.12 \end{vmatrix} \times \begin{vmatrix} 26.5 \\ \\ 63.0 \end{vmatrix} = \begin{vmatrix} 5.3 \\ \\ 7.6 \end{vmatrix} \text{ ft/sec}$$

The resulting vector diagrams are shown in figure 14, and their comparison with predicted performance is discussed in the section Effect of Rotative Speed.

APPENDIX E

COMPUTATION OF KLEINSORGE OPERATING POINTS

The values of torque coefficient C_m and Reynolds number Re (π_a and π_c, respectively, in appendix B) for the 111-centimeter (43.7-in.) smooth-disk Kleinsorge water brake were computed at two operating points as follows:

$$N = \begin{vmatrix} 4700 \\ \\ 5150 \end{vmatrix} \quad \begin{matrix} \text{for } Q_q \text{ known} \\ \\ \text{for housing } p_t \text{ known} \end{matrix}$$

and

$$\frac{P}{\text{disk}} = \begin{vmatrix} 5840 \\ \\ 5760 \end{vmatrix} \text{ kW}$$

$$= \begin{vmatrix} 7830 \\ \\ 7725 \end{vmatrix} \text{ hp}$$

from figure 7.

$$a = 55.5 \text{ cm}$$

$$= 21.85 \text{ in. (or } 1.82 \text{ ft)}$$

$$\omega = \begin{vmatrix} 4700 \\ \\ 5150 \end{vmatrix} \frac{2\pi}{60} = \begin{vmatrix} 492 \\ \\ 540 \end{vmatrix} \text{ rad/sec}$$

$$\nu = 0.325\times10^{-6} \text{ m}^2/\text{sec}$$

$$= 3.5\times10^{-6} \text{ ft}^2/\text{sec}$$

$$\text{Re} = \frac{\omega a^2}{\nu} = \frac{\begin{vmatrix} 492 \\ \\ 540 \end{vmatrix} (55.5)^2\times10^6}{0.325\times10^4} = \begin{vmatrix} 4.68\times10^8 \\ \\ 5.13\times10^8 \end{vmatrix}$$

$$T = \frac{C_3 P}{N}$$

$$= \frac{9550 \begin{vmatrix} 5840 \\ 5760 \end{vmatrix}}{\begin{vmatrix} 4700 \\ 5150 \end{vmatrix}} = \begin{vmatrix} 11\ 860 \\ 10\ 700 \end{vmatrix} \text{ m-N}$$

$$= \frac{5252 \begin{vmatrix} 7830 \\ 7725 \end{vmatrix}}{\begin{vmatrix} 4700 \\ 5150 \end{vmatrix}} = \begin{vmatrix} 8750 \\ 7885 \end{vmatrix} \text{ ft-lb}$$

$$C_m = \frac{2gT}{\rho \omega^2 a^5}$$

$$= \frac{2 \begin{vmatrix} 11\ 860 \\ 10\ 700 \end{vmatrix}}{968 \begin{vmatrix} 492 \\ 540 \end{vmatrix}^2 (0.555)^5} = \begin{vmatrix} 0.00192 \\ 0.00143 \end{vmatrix}$$

$$= \frac{2(32.2) \begin{vmatrix} 8750 \\ 7885 \end{vmatrix}}{60.5 \begin{vmatrix} 492 \\ 540 \end{vmatrix}^2 (1.82)^5} = \begin{vmatrix} 0.00192 \\ 0.00143 \end{vmatrix}$$

These two points are shown in figure 14 and are discussed in the section Example Operating Point for Kleinsorge Water Brake.

APPENDIX F

COMPUTATION OF VELOCITY DIAGRAMS FOR THE KLEINSORGE WATER BRAKE

The calculation was made as follows, starting with no through flow. At $Re = 4.68\times10^8$ (N_k = 4700 rpm), $C_{m,D} = 0.00162$ (for $Q = 0$). Scaling C_m to account for the difference in disk diameter and disk speed by using the π_a term:

$$C_{m,k} = C_{m,D}\left[\frac{(\omega^2 a^5)_k}{(\omega^2 a^5)_D}\right]$$

where

$$a_k = 55.5 \text{ cm } (21.85 \text{ in.}, 1.82 \text{ ft})$$

$$a_D = 23.0 \text{ cm } (9.06 \text{ in.}, 0.756 \text{ ft})$$

$$\omega\left|\begin{matrix}k\\D\end{matrix}\right| = \frac{Re\nu}{a^2} = \frac{4.68\times10^8\times0.325}{10^6\left|\begin{matrix}0.555\\0.230\end{matrix}\right|^2} = \left|\begin{matrix}492\\2860\end{matrix}\right| \text{ rad/sec}$$

$$\frac{(\omega^2 a^5)_k}{(\omega^2 a^5)_D} = \left(\frac{492}{2860}\right)^2 \times \left(\frac{55.5}{23.0}\right)^5 = 2.405$$

Therefore,

$$C_{m,k} = 0.00162 \times 2.405 = 0.00390$$

This value for $C_{m,k}$ is for a fully submerged disk with no through flow. For the real case $C_{m,k} = 0.00192$. Therefore,

$$\left(\frac{C_m}{C_{m,X=1}}\right)_{Q=0} = \frac{0.00192}{0.00390} = 0.492$$

$$X = \left(\frac{d}{a}\right) = 0.11$$

and

$$k_o = \left(\frac{U_c}{\omega r}\right) = 0.425$$

from figure 13.

$$d = \left(\frac{d}{a}\right) \times a = 0.11 \times 55.5 = 6.1 \text{ cm}$$

$$= 0.11 \times 21.85 = 2.4 \text{ in.}$$

$$r_m = a - \left(\frac{d}{2}\right) = 55.5 - 3.1 = 52.4 \text{ cm}$$

$$= 21.85 - 1.2 = 20.6 \text{ in.} = 1.72 \text{ ft}$$

$$\omega r_m = 492 \times 0.524 = 258 \text{ m/sec}$$

$$= 492 \times 1.72 = 847 \text{ ft/sec}$$

$$U_c = \left(\frac{U_c}{\omega r_m}\right) \times \omega r_m = 0.425 \times 258 = 110 \text{ m/sec}$$

$$= 0.425 \times 847 = 360 \text{ ft/sec}$$

$$\frac{V_s}{\omega r_m} = |0.10|$$

from figure 3(b) for $Q = 0$, averaged between disk and housing wall.

$$V_s = \left(\frac{V_s}{\omega r_m}\right) \times \omega r_m = 0.10 \times 258 = 26 \text{ m/sec}$$

$$= 0.10 \times 847 = 85 \text{ ft/sec}$$

The resultant velocity diagram for no through flow is shown in figure 17(c). From the figure and from equations (11) and (12), the calculated torque transmitted from the disk to the core and from the core to the housing walls is compared as follows. Starting with a modified form of equations (11) and (12), as discussed in the sections entitled "Internal Flow Analysis" and "Effects of Rotative Speed,"

$$T_{d-c} = C_{10} C_m \rho r_m A_w (\Delta U_{d-c})^2$$

$$= C_{10}(0.00192)978(0.524)0.2033(148)^2 = 4380\ C_{10} \text{ m-N}$$

$$= C_{10}\left[(0.00192)\frac{61.1(1.72)2.165(487)^2}{32.2}\right] = 3200\ C_{10} \text{ ft-lb}$$

From equation (12) with no through flow

$$T_{c-w,e} + T_{c-w,t} = C_{10}\left[C_m \rho r_m A_{w,e}(\Delta U_{c-w\ e})^2 + C_m \rho r_t A_{w,t}(\Delta U_{c-w,t})^2\right]$$

$$= C_{10}\Big[(0.00204)978(0.524)0.2033(110)^2$$

$$+ (0.00200)978(0.555)0.108(116.5)^2\Big]$$

$$= C_{10}(2550 + 1580)\text{m-N} = 4130\ C_{10} \text{ m-N}$$

$$= C_{10}\left[(0.00204)\frac{61.1(1.72)2.165(360)^2}{32.2}\right.$$

$$\left. + (0.00200)\frac{61.1(1.82)1.15(382)^2}{32.2}\right]$$

$$= C_{10}(1880 + 1165)\text{ft-lb} = 3045\ C_{10} \text{ ft-lb}$$

where the following assumptions were made:

$$s_t = 3.05 \text{ cm } (1.2 \text{ in.})$$

$$U_{c,t} = \left(\frac{r_t}{r_m}\right) U_{c,m}$$

and where $C_{m,c\text{-}w,e}$ and $C_{m,c\text{-}w,t}$ were determined from a curve going through a value of C_m of 0.00192 in figure 14, having the same slope as Daily's curves, at values of Reynolds determined from

$$Re_{c\text{-}w,e} = 4.7 \times 10^8 \left(\frac{\Delta U_{c\text{-}w,e}}{\Delta U_{d\text{-}c}}\right)$$

$$Re_{c\text{-}w,t} = 4.7 \times 10^8 \left(\frac{\Delta U_{c\text{-}w,t}}{\Delta U_{d\text{-}c}}\right)$$

The value of C_{10} cannot be determined because the value of torque with no through flow at the Kleinsorge levels of Reynolds number is not known. However, it is seen from these numbers that the ratio of calculated torque transmitted from the disk to the core and from the core to the side and tip walls of the housing agree closely (within 5 percent). It is also noted that 60 percent of the torque transmitted to the housing is through the side walls and that the remaining 40 percent is through the tip wall.

Next, the effects of through flow are considered as follows:

$$\frac{Q}{\text{disk}} = \left(\frac{\frac{0.32 \text{ m}^3}{\text{sec}}}{11 \text{ disks}}\right) = 0.029 \text{ m}^3/\text{sec}$$

$$= \left(\frac{5080}{60} \times 7.48 \times 11 = 1.03 \text{ ft}^3/\text{sec},\ 461 \text{ gal/min}\right)$$

from flagged point on curve J of figure 7.

$$A_q = 2 \times 2\pi \times r_m \times s_{eff} \left(\text{where } s_{eff} = \frac{s}{s} \times a \times 0.75\right)$$

$$= 4\pi \times 0.524 \times 0.055 \times 0.555 \times 0.75 = 152 \text{ m}^2$$

$$= 4\pi \times 1.72 \times 0.055 \times 1.82 \times 0.75 = 1.62 \text{ ft}^2$$

$$V_q = \left(\frac{Q}{A}\right)_q = \frac{0.029}{0.152} = 0.191 \text{ m/sec}$$

$$= \frac{1.03}{1.62} = 0.63 \text{ ft/sec}$$

Assume, as a first iteration,

$$d = 5.08 \text{ cm (2 in.)}$$

Therefore,

$$r_m = 52.8 \text{ cm (20.8 in. or 1.74 ft)}$$

$$U_{d,m} = r_m \omega = 0.528 \times 492 = 260 \text{ m/sec}$$

$$= 1.74 \times 492 = 856 \text{ ft/sec}$$

The effect that the incoming flow has on the core velocity is found through a momentum balance:

$$Q_c = (UA)_{c,q=0}$$

$$= \frac{110 \times 2.54 + 5.08}{10^4} = 0.142 \text{ (m}^3\text{/sec)/side}$$

$$= \frac{360 \times 1.0 \times 2}{144} = 5.0 \text{ (ft}^3\text{/sec)/side}$$

where $A_c = s_m \times d$, and $s_m = 2.54$ cm (1.0 in.).

$$U_c = \frac{(QU)_{c,q=0} + (QU)_q}{Q_c + Q_q} = \frac{0.284 \times 110 + 0.029 \times 0}{0.284 + 0.029} = 100 \text{ m/sec}$$

$$= \frac{10.0 \times 360 + 1.03 \times 0}{10.0 + 1.03} = 327 \text{ ft/sec}$$

$$k_o = \left(\frac{U_c}{U_d}\right)_m = \frac{100}{260} = 0.385$$

The resultant disk and wall vector diagrams with through flow are shown in figures 17(a) and (b). The torque balance between the disk and core and between the core and housing walls cannot be calculated from the diagrams, as was done previously with no through flow. To do so requires knowledge of C_7 in the solution of equations (11) and (12).

Using the relation between C_m and ΔU_{d-c} determined in the section entitled Effects of Through Flow, the water depth is determined as follows:

$$\frac{C_{m(\text{with } Q)}}{C_{m(Q=0)}} = \left(\frac{\Delta U_{(\text{with } Q)}}{\Delta U_{(Q=0)}}\right)_{d-c} = \frac{529}{487} = 1.09$$

then X (which is d/a) becomes:

$$\left(\frac{C_m}{C_{m,X=1}}\right)_{(\text{with } Q)} = \frac{0.492}{1.09} = 0.45$$

$$X = 0.095$$

from figure 13.

$$d = \left(\frac{d}{a}\right) \times a = 0.095 \times 55.5 = 5.28 \text{ cm}$$

$$= 0.095 \times 21.85 = 2.08 \text{ in.}$$

$$r_m = a - \left(\frac{d}{2}\right) = 55.5 - 2.6 = 52.9 \text{ cm}$$

$$= 20.8 \text{ in.}, \ 1.735 \text{ ft}$$

The core rotational speed coefficient k_o is then computed at the operating point where the housing pressure is known from the dimensions noted in figure 17(d) and equation (9) for pressure:

$$\frac{\Delta p}{\Delta r} = C_6 \rho \frac{(U_c)^2}{r_m}$$

where

$$U_c = k_o U_{m,d} = k_o \times \omega r_m = k_o \times 540 \times 0.529 = 286 \ k_o \text{ m/sec} \ (k_o \times 540 \times 1.735 = 937 \ k_o \text{ ft/sec})$$

and

$$\Delta r = d$$

$$\frac{\Delta p}{d} = \frac{978(286 \ k_o)^2}{1000(0.524)} = 152(k_o)^2 \text{ N/cm}^3$$

$$= \frac{61.1(937 \ k_o)^2}{1728(32.2)1.72} = 560(k_o)^2 \text{ lb/in.}^3$$

$$\Delta p = \left(p_{out} - p_{in}\right)_c = (141 - 10) = 131 \text{ N/cm}^2$$

$$= 205 - 15 = 190 \text{ lb/in.}^2$$

where the housing is assumed vented to atmosphere. Combining these equations yields

$$k_o = \sqrt{\frac{\Delta p}{152d}} = \sqrt{\frac{131}{152 \times 5.28}} = 0.404 \ \text{(for SI units)}$$

$$= \sqrt{\frac{\Delta p}{560d}} = \sqrt{\frac{190}{560 \times 2.08}} = 0.404 \ \text{(for U.S. customary units)}$$

The results of these calculations are discussed in the section Example Operating Point for Kleinsorge Water Brake.

REFERENCES

1. Schlichting, Hermann (J. Kestin, trans.): Boundary Layer Theory. Fourth ed., McGraw-Hill Book Co., Inc., 1960.

2. Daily, J. W.; Ernst, W. D.; and Asbedian, V. V.: Enclosed Rotating Disks with Superimposed Throughflow: Mean Steady and Periodic Unsteady Characteristics of the Induced Flow. Rep. 64-16, Massachusetts Inst. Tech. (AROD-2500-2, AD-443060), Apr. 1964.

3. Watabe, Komei: Effects of Clearances and Grooves on Fluid Friction of Rotating Discs. Bull. JSME, vol. 8, no. 29, Feb. 1965, pp. 55-63.

4. Deavers, C. J.: Water Brake Dynamometer. Rep. R51GL106-1, General Electric Co., Jan. 1952.

5. Ketola, H. N.; and McGrew, J. M.: Theory of the Partially Wetted Rotating Disks. Paper H4, British Hydromechanics Research Association 3rd International Conference on Fluid Sealing, Cambridge England, Apr. 3-5, 1967.

6. Wosika, Leon R.: Direct Drive Viscous Shear Water Dynamometers for Large Gas Turbines. Paper 710216, SAE, Jan. 1971.

TABLE I. - SUMMARY OF DATA

Source	Disk diameter		Through flow	Power to through-flow rate ratio		Reynolds number	Axial spacing ratio, s/a	Disk submergence	Disk surface	Housing surface	Fluid
	cm	in.		kW-sec/m^3	hp-sec/ft^3						
Kleinsorge	14.0 - 133.1	5.5 - 52.4	Yes	440	16.7	$(10 - 1000)10^6$	0.055	Partial	Smooth	Smooth	Water
Ref. 2	46.0	18.1	Yes	Range	Range	$(1.7 - 8)10^6$	[a].069	Full	Smooth	Smooth	Air, water
Ref. 3	22.6	8.9	No	-----	-----	$(0.004 - 3)10^6$	[a].029, .089, .177	Full	Smooth-grooved	Smooth-grooved	Water
Ref. 4	14.0	5.5	Yes	292	11.1	$(17 - 34)10^6$	.111	Range	Smooth	Smooth	Water
Ref. 5	----------	----------	No	-----	-----	----------	[a].05	Range	Smooth	Smooth	---------
Ref. 6	20.3	8.0	Yes	Range	Range	49×10^6	.06	Range	Smooth	Smooth	Water

[a]Arbitrarily selected from range covered in reference.

TABLE II. - MATRIX OF DIMENSIONLESS PI TERMS

π	τ	ρ	ν	ΔU (a)	a	λ (b)	ω	D	T	g	A	σ	e	Q	Δp	p	V (c)	P	Pi terms
	C_1	C_2	C_3	C_4	C_5	C_6	C_7	C_8	C_9	C_{10}	C_{11}	C_{12}	C_{13}	C_{14}	C_{15}	C_{16}	C_{17}	C_{18}	
1	1				2			-1											$(\tau a^2/D)$
2		1			-2			-1						2					$(\rho Q^2/a^2D)$
3			1		1									-1					$(\nu a/Q)$
4				1	2									-1					$(\Delta U a^2/Q)$
5					-1			-1	1										(T/aD)
6					-1	1													(λ/a)
7					3		1							-1					$(\omega a^3/Q)$
8					5					1				-2					$(a^5 g/Q^2)$
9					-2						1								(A/a^2)
10					1			-1				1							$(a\sigma/D)$
11					2			-1					1						(ea^2/D)
12					2			-1							1				$(\Delta p a^2/D)$
13				-1													1		$(\dot{V}/\Delta U)$
14															1	-1			$(\Delta p/p)$
15					2			-1						-1				1	(Pa^2/QD)

[a]ΔU can be ΔU_{d-c}, ΔU_{c-w}, U_d, etc.
[b]λ can be s, d, r, etc.
[c]V can be V_s, V_q, U, etc.

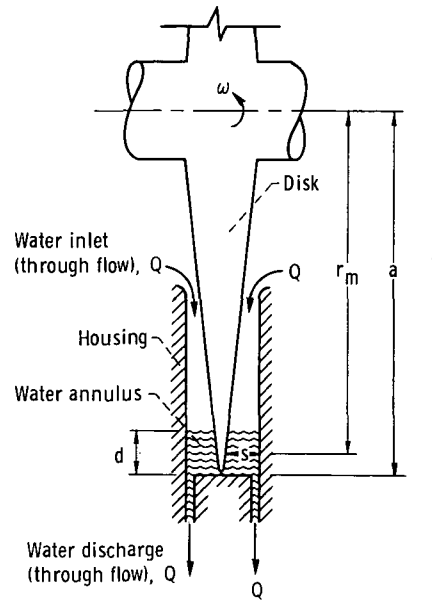

Figure 1. - Cross section of smooth-disk water brake.

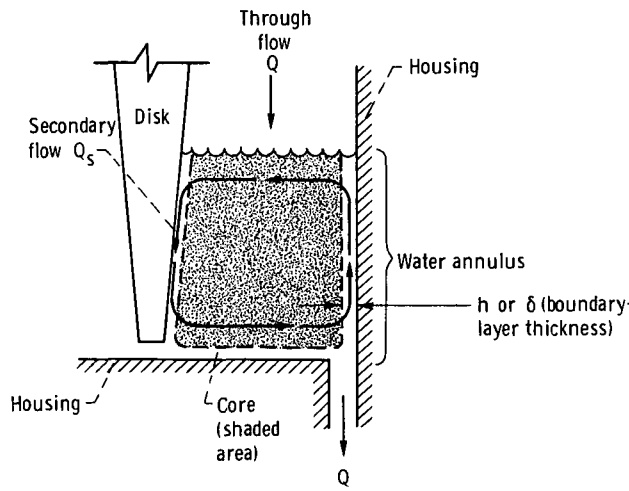

Figure 2. - Cross-section of water annulus on one side of disk showing boundary layer, core, through flow, and secondary flow.

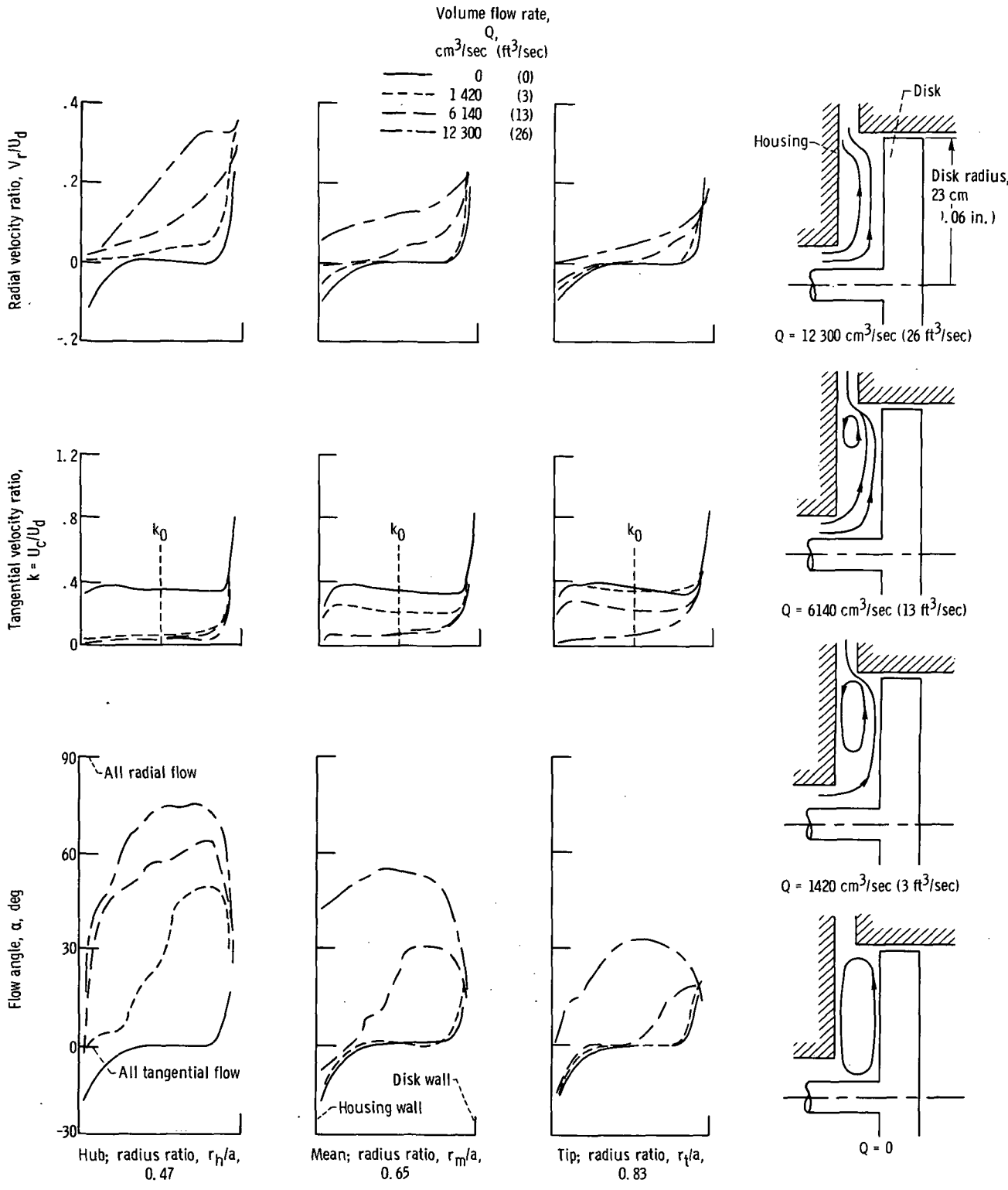

(a) Low Reynolds number ($Re = 2.9 \times 10^5$).

Figure 3. - Measured flow velocity ratios and flow angles for enclosed smooth disk rotating in air. Data from reference 2 for flow regime IV. Axial spacing ratio, 0.069.

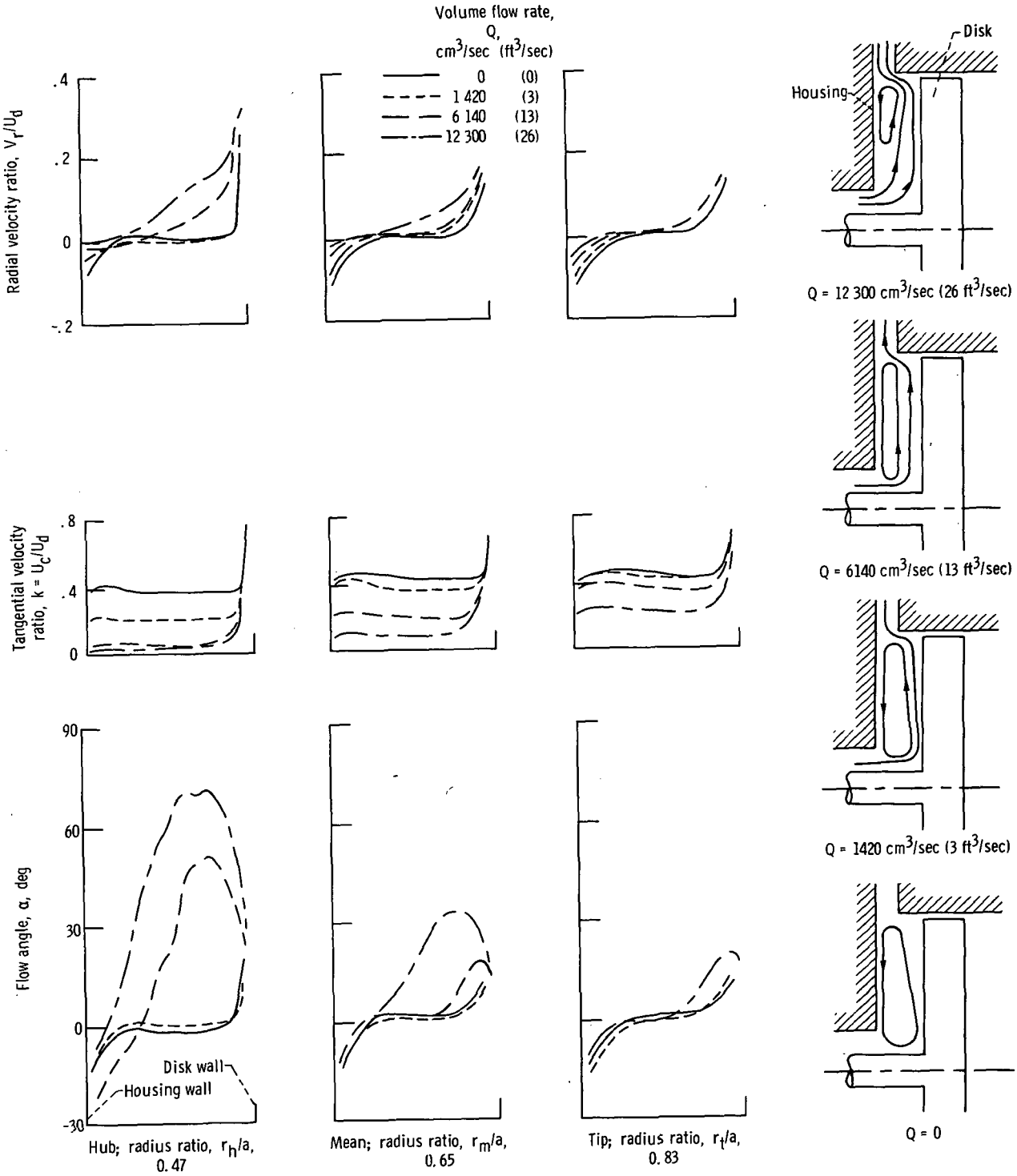

(b) High Reynolds number (Re = 6.9×10^5).

Figure 3. - Concluded.

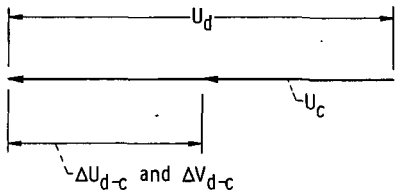

(a) Disk.

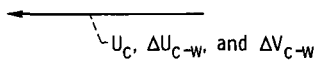

(b) Housing wall.

Figure 4. - Vector diagram for rotating core flow (no through flow or secondary flow) at mean radius of water annulus.

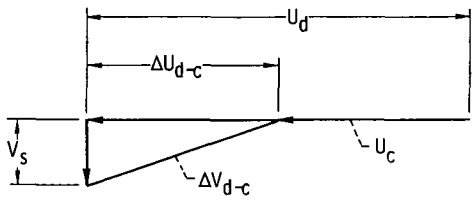

(a) Disk.

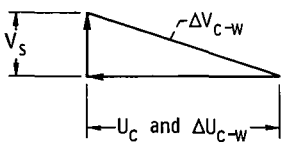

(b) Housing wall.

Figure 5. - Vector diagram for rotating core flow with superimposed secondary flow at mean radius of water annulus.

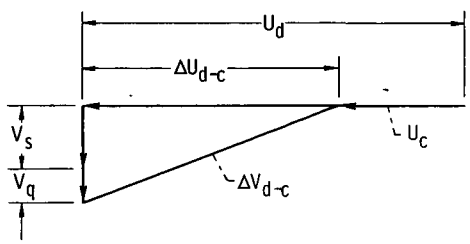

(a) Disk.

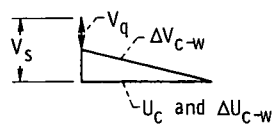

(b) Housing wall.

Figure 6. - Vector diagrams for rotating core flow with superimposed secondary and through flow at mean radius of water annulus.

○ Maximum power points
△ Part power points
ⵔ See supplementary note

Curve	Data	Number of disks	Diameter, cm	Diameter, (in.)	Supplementary notes
a	Deavers	1	14.0	(5.5)	Axial spacing ratio, 0.111
b	*Kleinsorge*	3	14.0	(5.5)	----------
c		11	18.5	(7.28)	----------
d		4	32.0	(12.6)	----------
e		8	32.0	(12.6)	----------
f		4	40.0	(15.75)	----------
g		11	71.0	(27.95)	----------
h		3	111.0	(43.7)	Axial spacing ratio, 0.050 to 0.056; Water pressure, 141 N/cm^2 (205 lbf/in.^{2}) at housing radius a
i		3	111.0	(43.7)	Axial spacing ratio, 0.050 to 0.056
j		11	111.0	(43.7)	Water through flow, 0.32 m^3/sec (5080 gal/min)
k		10	133.0	(52.4)	----------

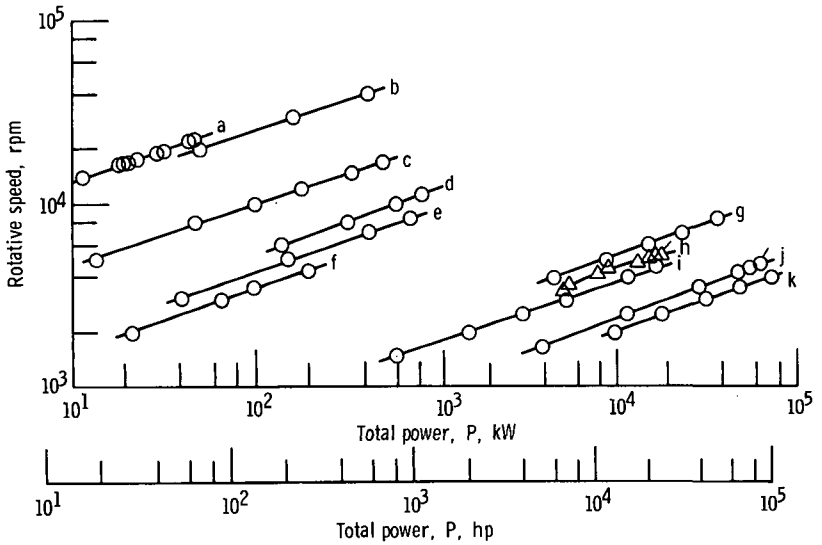

Figure 7. - Power curves for single disk and multidisk water brakes. All disks partially submerged in water except for Deavers' data (ref. 4).

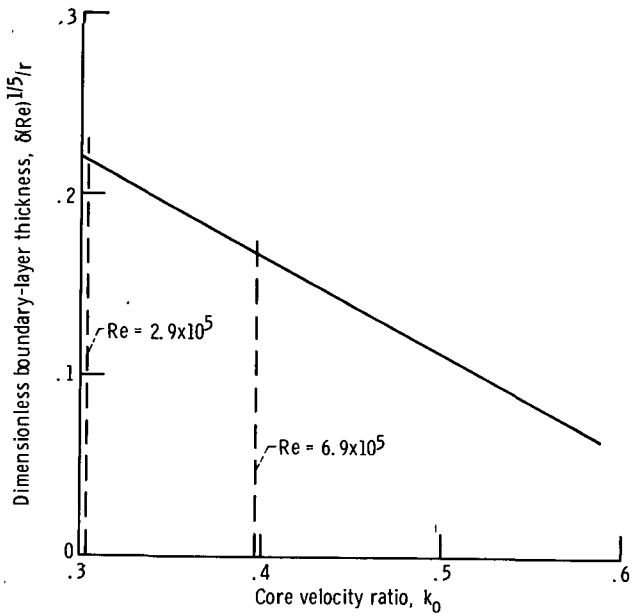

Figure 8. - Boundary-layer thickness as function of core rotational speed (from fig. 41 of ref. 2). (Re values are from appendix D.)

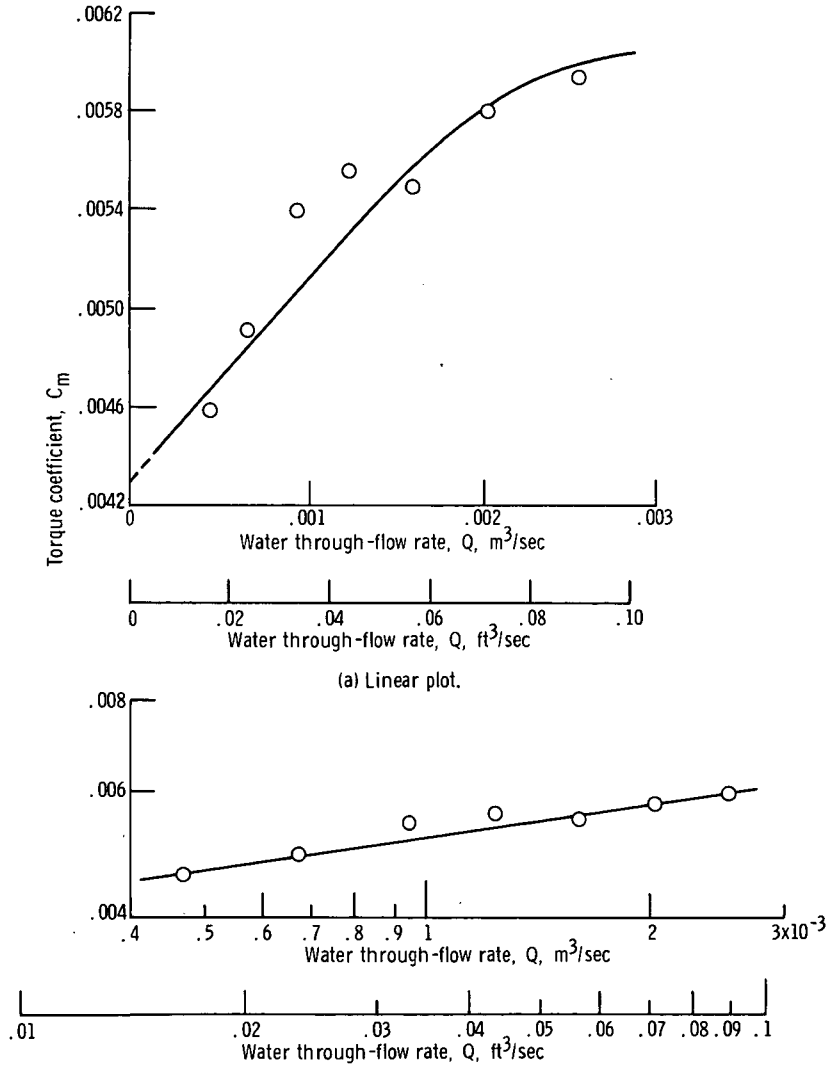

(a) Linear plot.

(b) Logarithmic plot.

Figure 9. - Effect of water through-flow rate on torque coefficient; Reynolds number, $2.4x10^6$. Data from reference 2 for disk fully submerged in water.

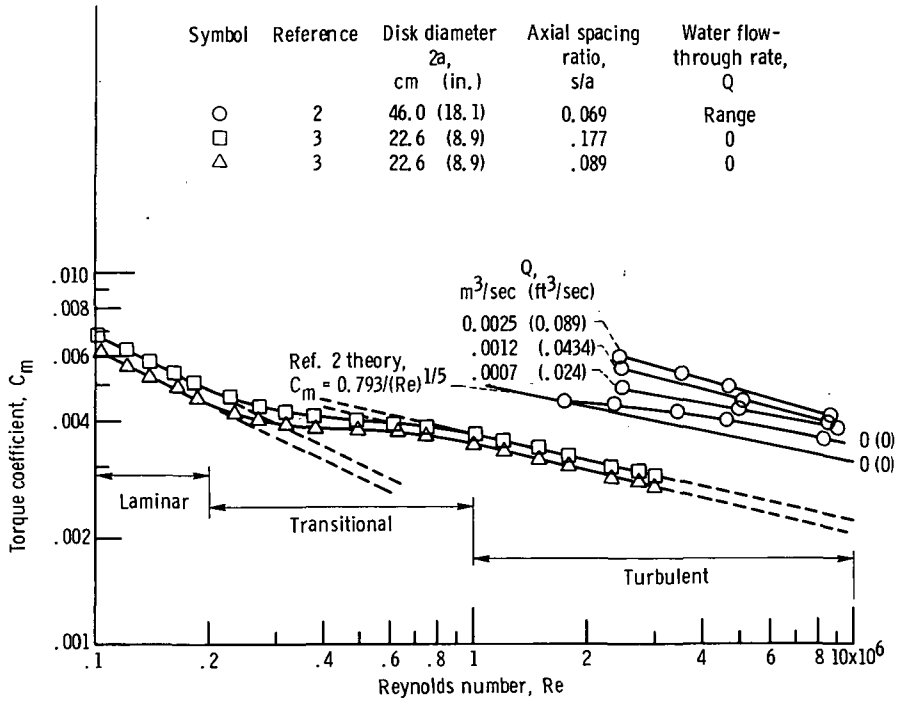

Figure 10. - Effect of Reynolds number (rotative speed) on torque coefficient for smooth disks fully submerged in water.

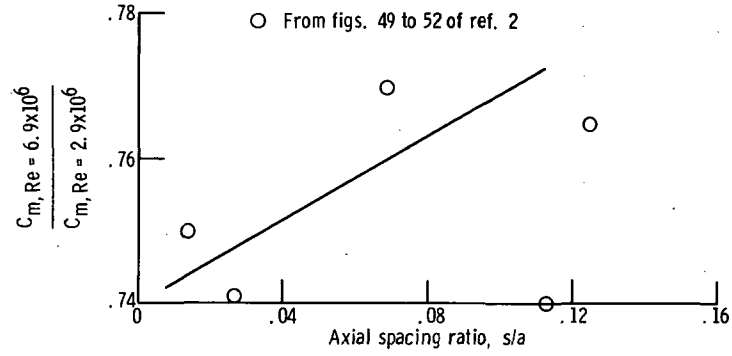

Figure 11. - Effect of axial spacing between disk and housing wall on ratio of torque coefficient between two speeds ($Re = 2.9x10^6$ and $6.9x10^6$). Through-flow rate, 0.0025 cubic meters per second (0.089 ft^3/sec).

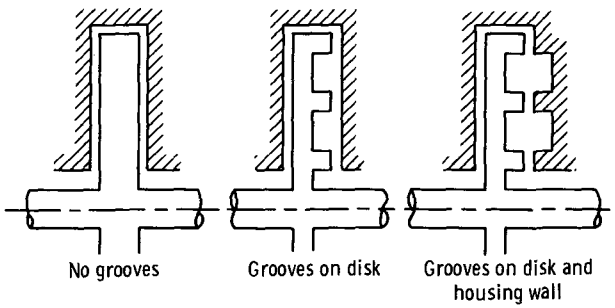

(a) Reference 3 disk and housing wall configuration.

Symbol	Reference	Disk diameter, 2a, cm (in.)	Axial spacing ratio, s/a	Water through-flow, Q
——	3	22.6 (8.9)	0.029	No
O	4	14.0 (5.5)	.111	Yes

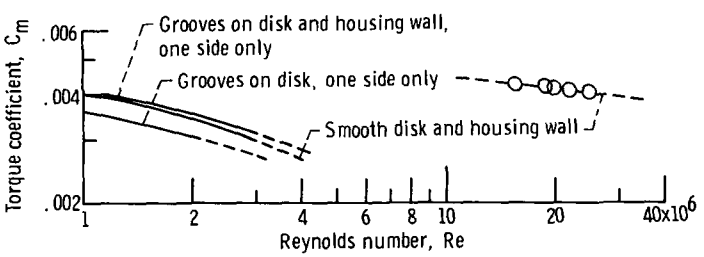

(b) Torque coefficient as function of Reynolds number.

Figure 12. - Effect of grooves and Reynolds number (rotative speed) on torque coefficient for disk fully submerged in water.

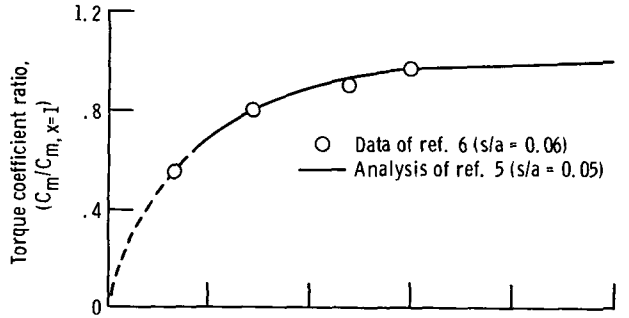

(a) Torque coefficient.

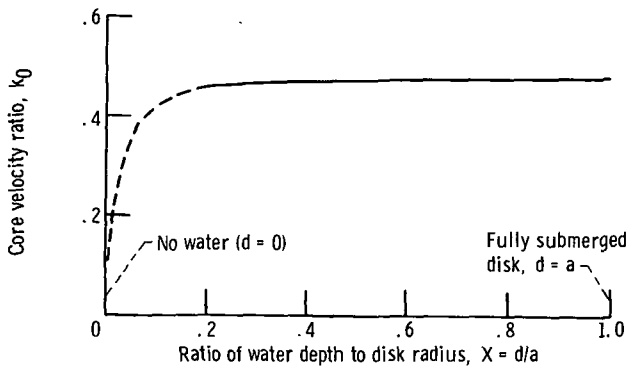

(b) Core rotational velocity ratio.

Figure 13. - Effect of submergence on torque coefficient and core rotational velocity ratio.

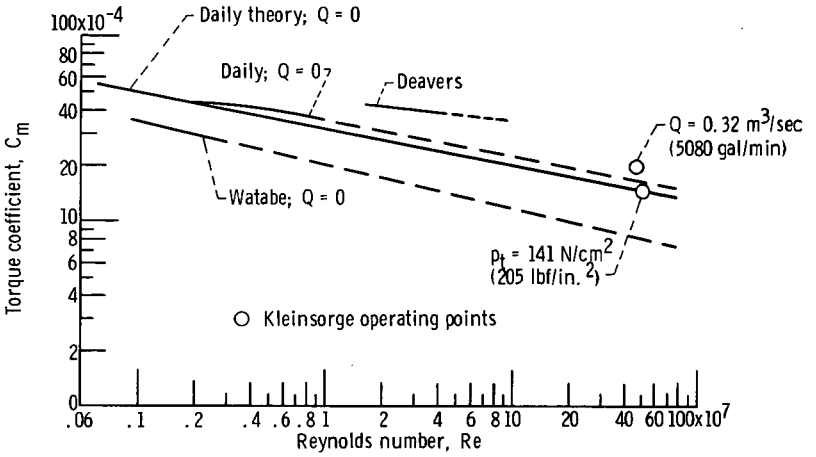

Figure 14. - Predicted torque coefficients at extrapolated or calculated values of Reynolds number for smooth disks in water.

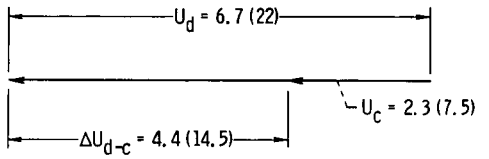

(a) Water through flow rate, 0.

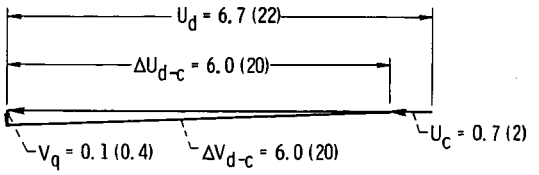

(b) Water through flow rate, 0.0028 cubic meter per second (0.10 ft³/sec).

Figure 15. - Mean radius disk vector diagrams showing effect of through flow, computed for smooth disk of reference 2 (see appendix C). (Velocities are in m/sec (ft/sec).)

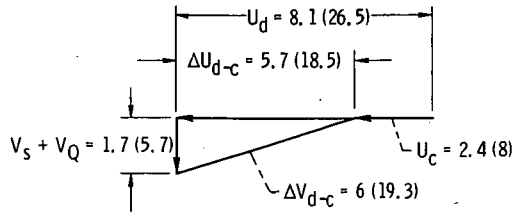

(a) Reynolds number, 2.9×10^6.

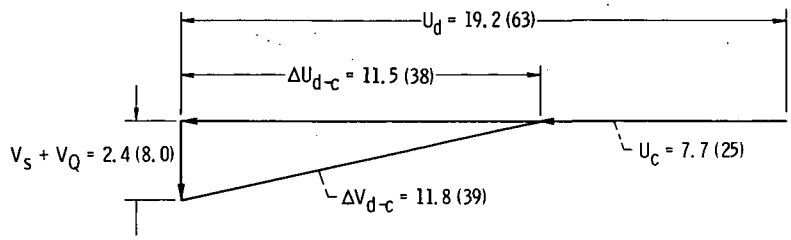

(b) Reynolds number, 6.9×10^6.

Figure 16. - Mean radius disk vector diagrams for smooth disk of reference 2 at two rotative speeds (Reynolds numbers). Water through flow rate, 0.0025 cubic meter per second (0.089 ft^3/sec). (Velocities are in m/sec (ft/sec). Calculations are in appendix D.)

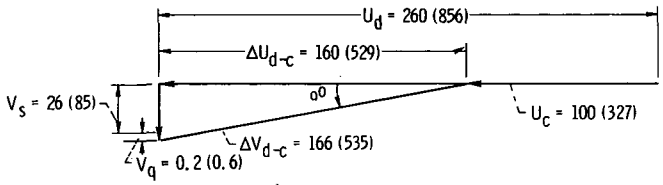

(a) Disk wall; water brake operating with through flow; water depth, 5.28 centimeters (2.08 in.).

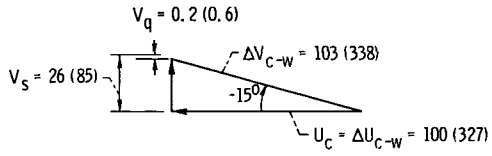

(b) Housing wall; water brake operating with through flow; water depth, 5.28 centimeters (2.08 in.).

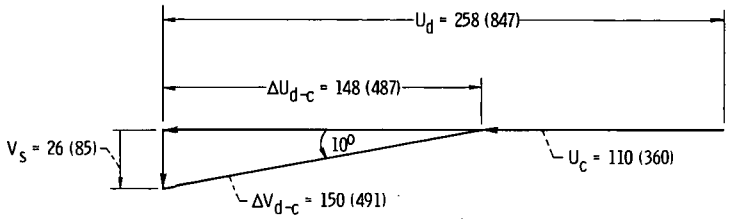

(c) Disk wall; water brake operating with no through flow; water depth, 6.1 centimeters (2.4 in.).

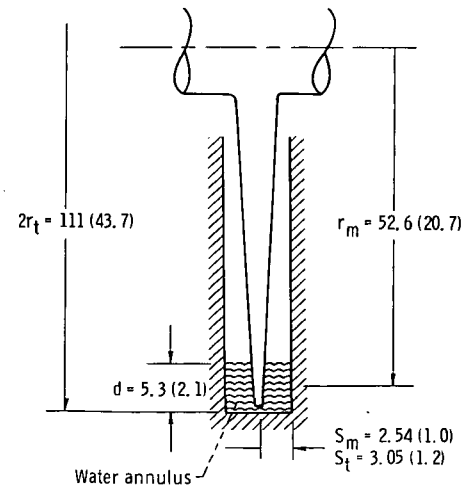

(d) Dimensional model when operating with through flow.

Figure 17. - Vector diagrams at mean radius of water annulus computed for the 111-centimeter (43.7-in.) Kleinorge water brake operating at 4700 rpm. (Velocities are in m/sec (ft/sec). Calculations are in appendix F.)

Page Intentionally Left Blank

NATIONAL AERONAUTICS AND SPACE ADMINISTRATION
WASHINGTON, D.C. 20546

OFFICIAL BUSINESS
PENALTY FOR PRIVATE USE $300

SPECIAL FOURTH-CLASS RATE
BOOK

POSTAGE AND FEES PAID
NATIONAL AERONAUTICS AND
SPACE ADMINISTRATION
451

U.S.MAIL

POSTMASTER: If Undeliverable (Section 158 Postal Manual) Do Not Return

"The aeronautical and space activities of the United States shall be conducted so as to contribute . . . to the expansion of human knowledge of phenomena in the atmosphere and space. The Administration shall provide for the widest practicable and appropriate dissemination of information concerning its activities and the results thereof."

—NATIONAL AERONAUTICS AND SPACE ACT OF 1958

NASA SCIENTIFIC AND TECHNICAL PUBLICATIONS

TECHNICAL REPORTS: Scientific and technical information considered important, complete, and a lasting contribution to existing knowledge.

TECHNICAL NOTES: Information less broad in scope but nevertheless of importance as a contribution to existing knowledge.

TECHNICAL MEMORANDUMS: Information receiving limited distribution because of preliminary data, security classification, or other reasons. Also includes conference proceedings with either limited or unlimited distribution.

CONTRACTOR REPORTS: Scientific and technical information generated under a NASA contract or grant and considered an important contribution to existing knowledge.

TECHNICAL TRANSLATIONS: Information published in a foreign language considered to merit NASA distribution in English.

SPECIAL PUBLICATIONS: Information derived from or of value to NASA activities. Publications include final reports of major projects, monographs, data compilations, handbooks, sourcebooks, and special bibliographies.

TECHNOLOGY UTILIZATION PUBLICATIONS: Information on technology used by NASA that may be of particular interest in commercial and other non-aerospace applications. Publications include Tech Briefs, Technology Utilization Reports and Technology Surveys.

Details on the availability of these publications may be obtained from:

SCIENTIFIC AND TECHNICAL INFORMATION OFFICE

NATIONAL AERONAUTICS AND SPACE ADMINISTRATION

Washington, D.C. 20546